NASA CONTRACTOR REPORT 166530

INVESTIGATION OF IMAGE ENHANCEMENT TECHNIQUES FOR THE DEVELOPMENT OF A SELF-CONTAINED AIRBORNE RADAR NAVIGATION SYSTEM

Anil V. Phatak
Mehebub S. Karmali

CONTRACT NAS2- 11276
July 1983

NASA

NASA CONTRACTOR REPORT 166530

INVESTIGATION OF IMAGE ENHANCEMENT TECHNIQUES FOR THE DEVELOPMENT OF A SELF-CONTAINED AIRBORNE RADAR NAVIGATION SYSTEM

Anil V. Phatak
Meheubu S. Karmali

Prepared for
Ames Research Center
under Contract NAS2-11276

National Aeronautics and
Space Administration

Ames Research Center
Moffett Field, California 94035

TABLE OF CONTENTS

ABSTRACT

This study was devoted to an investigation of the feasibility of applying advanced image processing techniques to enhance radar image characteristics that are pertinent to the pilot's navigation and guidance task. Millimeter (95 GHz) wave radar images for the overwater (i.e., offshore oil rigs) and overland (Heliport) scenario were used as a data base. The purpose of the study was to determine the applicability of image enhancement and scene analysis algorithms to detect and improve target characteristics (i.e., man-made objects such as buildings, parking lots, cars, roads, helicopters, towers, landing pads, etc.) that would be helpful to the pilot in determining his own position/orientation with respect to the outside world and assist him in the navigation task.

Results of this study show that significant improvements in the raw radar image may be obtained using two dimensional image processing algorithms. In the overwater case, it is possible to remove the ocean clutter by thresholding the image data, and furthermore to extract the target boundary as well as the tower and catwalk locations using noise cleaning (e.g., median filter) and edge detection(e.g., Sobel operator) algorithms. Similarly, overland images may be processed using nonlinear contrast stretching and line feature extraction algorithms to produce an image where buildings, parking lot boundaries and helicopters on the ground may be identified by a trained operator.

PREFACE

This effort was performed under contract No. NAS2-11276 from the NASA Ames Research Center. Dr. John S. Bull was the Technical Monitor for this project.

The project manager at Analytical Mechanics Associates, Inc. (AMA) was Dr. Anil V. Phatak. The AMA project engineer was Mr. Mehebub S. Karmali. Dr. Anil K. Jain, the consultant on this project, made significant technical contributions to this research effort, particularly in providing guidance in the selection of the image enhancement algorithms for application to the overland radar data. The assistance of Mr. George Clary of NASA throughout this project is gratefully acknowledged.

1. INTRODUCTION

The helicopter's unique operating characteristics and ability to circumvent time delays of other modes of transportation has led to significant increases in civilian use. Continued expansion of civilian helicopter applications requires all-weather capability.

Current helicopter IFR operations are generally limited to landing fields having expensive electronic navigational aids, which includes less than 3 percent of the landing facilities in the United States. This situation discourages operations at small utility fields, landing pads in remote areas, off-shore oil platforms, and unpredictable locations of emergency rescue operations. Consequently, there is a growing need to develop an onboard navigation and guidance system which can operate independently of ground facilities and does not require an electronic aid installed at each landing site. The resulting "self-contained" guidance and navigation system would add greater freedom and flexibility to helicopter operation in all types of weather. Such a system would also benefit the corporate operator who desires lower instrument approach minimums than offered by RNAV, but who is unable to afford the installation of precision ground navigation aids.

1.1 Background

A system using imaging radar is a promising candidate for use as a self-contained airborne navigation system. However, at the present time, the use of airborne radar as a navigation aid is limited primarily to remote offshore operations. Widespread utilization of such image-based navaids for other scenarios under all-weather conditions is restricted due to limitations that are inherent to the present state of the system hardware/software implementation and to the operational procedures in current use.

The hardware limitations relate to the radar system parameters such as the frequency ($9 \sim 100$ GHz), the pulse repetition frequency (PRF), and the antenna gain pattern. Software limitations depend upon the sophistication of the on-board processing algorithms applied to the raw radar image data. Image

processing/enhancement algorithms offer a software alternative to improving the quality of the radar image display for navigation and guidance applications.

This report describes the results of a study devoted towards investigating the feasibility of improving the quality of the displayed radar image (from a navigation and guidance viewpoint) by applying advanced image processing and scene analysis algorithms to the raw radar image data. Millimeter wave (95 GHz) radar images for the overwater and overland scenarios were used as the data base for testing the image enhancement techniques.

1.2 Objectives

The objectives of this research study were twofold:

1. Identify, define and characterize radar video image characteristics that are pertinent to the pilot's navigation task requirements. That is, image characteristics corresponding to natural features (such as rivers, ridges, mountains, lakes) or man-made object features (like runways, helipads, oil rigs, roads, buildings) that may be used by the pilot to determine aircraft position with respect to earth referenced coordinates.

2. Determine the feasibility of applying advanced image enhancement/scene analysis algorithms to identify and enhance image characteristics that are useful in real time applications for flight guidance and navigation.

1.3 Report Outline

This report is organized into six sections. Section 2 gives a description of the radar image data used in this study for testing the capability of candidate-image enhancement techniques. A self-contained summary and review of image processing/enhancement algorithms are provided in Section 3, in the interest of completeness. Results of applying selected image enhancement

techniques to overwater and overland radar images are presented in Sections 4 and 5, respectively. Conclusions and recommendations for further work are summarized in Section 6.

2. DESCRIPTION OF RADAR IMAGE DATA

Radar image data provided by the NASA-Ames Research Center was used in this study effort. A description of the physical scenario/imaging geometry, radar characteristics, data format and actual radar images is provided i the following paragraphs.

2.1 Physical Scenario/Imaging Geometry

Two physical scenarios were used to gather the radar image data: (1) an overwater oil rig scenario off the Louisiana coast in the Gulf of Mexico, and (2) an overland site, at the Petroleum Helicopters, Inc. (PHI) heliport in Venice, Louisiana. Color photographic prints of these two test sites are shown in Figures 1 and 2, respectively.

A 95 GHz radar sensor (developed by Norden Systems, Inc.), mounted in the cargo bay of a helicopter in the side-looking mode, was flown over the above two test sites to gather a sequence of frames of radar video images. Figure 3

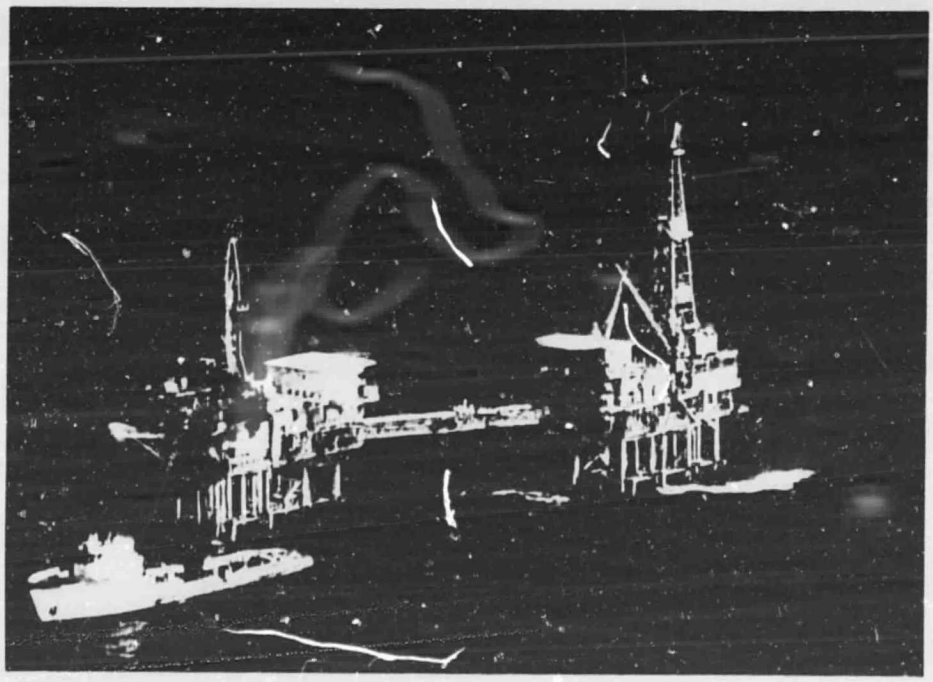

Figure 1. Overwater Oil Rig Scenario

ORIGINAL PAGE
COLOR PHOTOGRAPH

Figure 2. Overland PHI Heliport Site

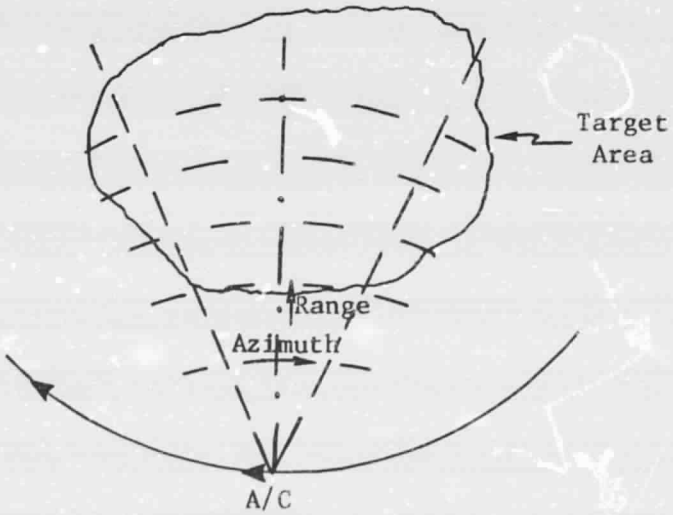

Figure 3. Radar Imaging Geometry

shows a sketch of the imaging geometry for these flight tests. The aircraft was flown at altitudes of 150 m to 300 m and an airspeed of approximately 60 knots in a clockwise circular trajectory of 500 m to 1000 m radius around the target region (i.e., oil rig or PHI heliport).

2.2 Radar Characteristics

The parameters characterizing the Norden millimeter wave radar are given in Table 1.

Table 1. Radar Parameters

Parameter	Specified Value	Actual Value
Frequency	95 GHz (Nom)	-
Azimuth Beamwidth	0.33 deg. (63 cm antenna)	-
Elevation Pattern	$\csc^2\cos^{1/2}$	-
Polarization	Alternating Horizontal/ Vertical	-
Pulse Width	50 ns	-
Pulse Repetition Frequency (PRF)	2 KHz	
Scan Width	Analog Adjustable to $\pm$ 22.5°	+18.5, -15.5 deg
Scan Speed	20 deg/s	~24 deg/s

The actual resolution of the radar is 7.5 meters in range and 0.33 degrees in azimuth.

2.3 Image Data Description

Radar video images consisting of a sequence of single frames, in the format shown in Figure 4, were used as the experimental data base in this study. Each frame consists of 206 rows and 2860 columns corresponding to a

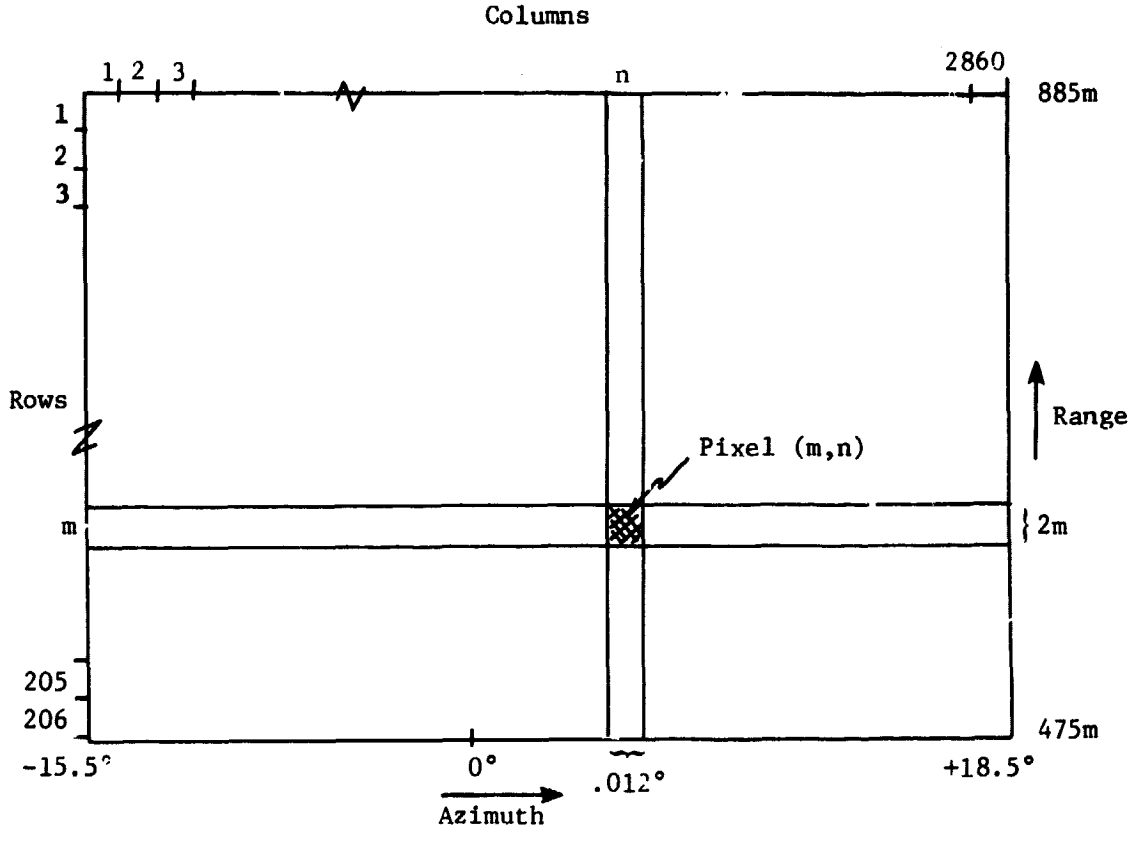

Figure 4. Data Format of Single Image Frame

region covering (475-885) meters in range and (-15.5 - +18.5) degrees in azimuth, respectively. Pixel image intensity is represented on a 6-bit

($L = 2^6 = 64$ grey levels) scale. Each column consists of radar returns at a particular azimuth angle for a single pulse. Each row corresponds to radar returns at a given slant range. Furthermore, radar pulses have an alternating horizontal/vertical polarization. Thus, for a single frame, all the even columns have one polarization, and all the odd columns the alternate polarization.

Note that the raster image format of Figure 4 represents a nonlinear transformation of the raw radar image from a polar (ρ , θ) format to a cartesian (x,y) coordinate frame. As a result, bin size along the azimuth axis varies from 0.1 m at the nearest range of 475 m to 0.185 m at the farthest range of 885 m, for an average horizontal bin width of .14 m at midrange. The bin size along the range axis is 2 m. During this study, raw radar images were smoothed along the azimuth axis by averaging groups of 5 successive columns with the horizontal or vertical polarization, or 10 consecutive columns of horizontal and vertical polarization. The result is a single smoothed image frame with 206 rows and 286 columns. Hereafter, images obtained by averaging five (5) consecutive even columns are labeled as even (E) images, those using sum of five (5) odd columns are called odd (O) images, and images obtained through averaging ten successive even and odd columns are referred to as sum (S) or even plus odd (E+O) images. The effect of column averaging on a given image is to reduce the noise clutter and thus increase the overall signal to noise ratio.

The averaging of alternating columns results in the bin size along the azimuth axis to vary from 1 m to 1.85 m. Assuming the average azimuth bin size to be 1.4m, the aspect ratio (range:azimuth) for a pixel is 2:1.4. By definition, a pixel on the display monitor has an aspect ratio of 1:1. This means that for the radar image to have the correct aspect ratio, the image has to be zoomed by a factor of 2 in the range direction and a factor of 1.4 in the azimuth direction. Since the image processing software allowed only integer zoom, the radar images were zoomed by a factor of 2 in the range direction and unchanged in the azimuth direction. Thus, each of the zoomed even, odd and sum radar images have 412 rows and 286 columns. Note that zooming in the range direction is achieved by repeating each row once.

2.4 Radar Video Images

A total of nineteen (19) radar images, nine (9) for the overwater oil rig scenarios of Figure 1, and ten (10) for the overland PHI heliport site shown in Figure 2 were available for this study. Figures 5 and 6 show examples of the sum (S) radar images for the overwater and overland cases, respectively. On examination of the radar and photographic images, it is apparent that the raw radar images for the two scenarios could be greatly improved through processing by image enhancement algorithms.

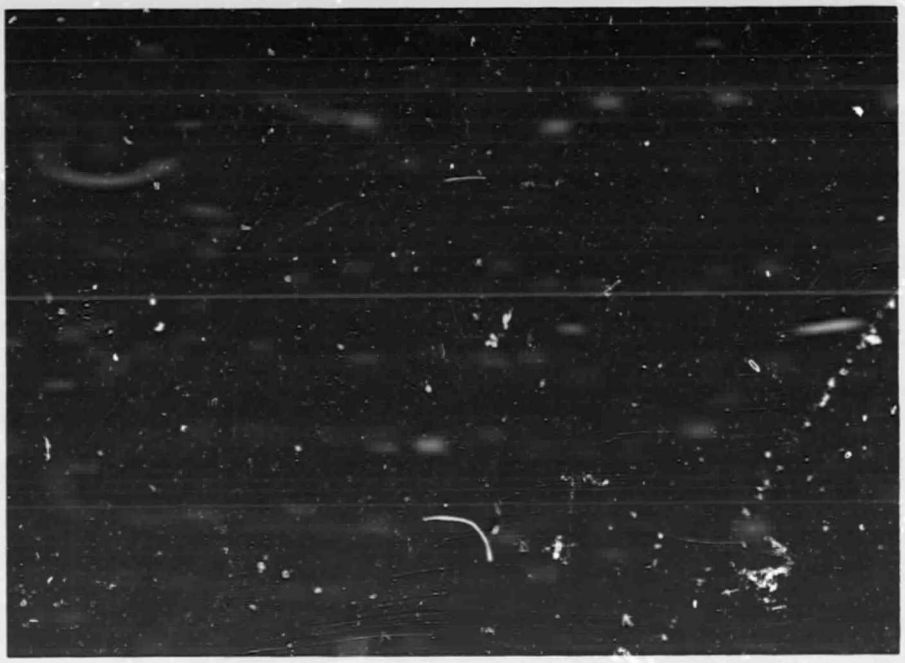

Figure 5. Overwater Sum Radar Image

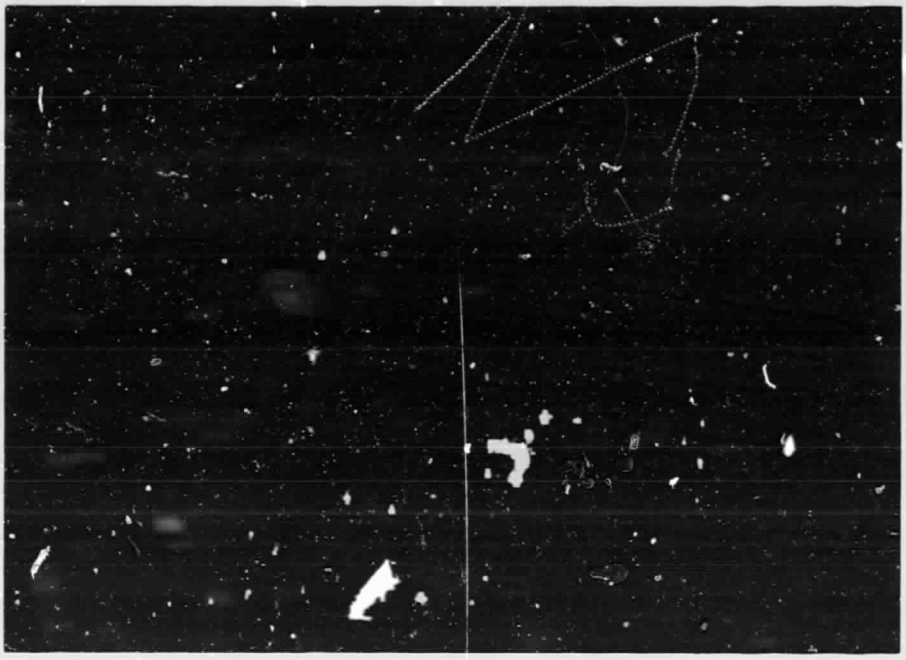

Figure 6. Overland Sum Radar Image

3. IMAGE ENHANCEMENT

The purpose of this study was to investigate the merits and feasibility of applying image enhancement/analysis techniques to process radar image data with a view towards improving the quality of the visual image from a pilot's flight navigation and guidance viewpoint. Unfortunately, image quality has a subjective connotation and depends ultimately upon the context within which an image is being examined. As a result, it is not possible at the outset to prescribe a structured approach towards selecting the best image enhancement operations for any new set of image data. Instead, what is available to the research investigator is a set of organized tools for manipulating and processing two-dimensional images. Evaluation of the image enhancement schemes must be based upon subjective assessment of image quality improvements obtained after processing the raw image data.

The purpose of this section is to provide a comprehensive description of the individual or primitive image processing operations that may be useful for constructing and implementing real-time radar image enhancement algorithms. The following three types of operations are described: (1) Point operations, (2) Spatial operations, and (3) Edge detection operations. References [1]-[5] provide excellent material describing these operations in more detail.

3.1 Point Operations

Point operations involve the modification of the image intensity distribution and contrast on a pixel-by-pixel basis. Thus, given a raw input image $\{u(m,n): 0 \leq m \leq M, 0 \leq n \leq N\}$, where u is the grey level ($0 \leq u \leq L = 2^n$: n bit scale) of pixel (m,n), the point operation defined by the transformation:

$$v(m,n) = f\{u(m,n)\}$$

modifies the grey level values of each pixel and hence changes the image contrast of the overall image. The choice of the function f allows considerable flexibility in image contrast manipulation. Some of the frequently-used operations are described below.

3.1.1 Scaling Operations

An n bit display monitor can only show pixel integer grey levels in the range 0 to 2^n. Thus, for an 8 bit display, pixel intensities assume integer values between 0 and 255. However, raw input images may not occupy the same dynamic range of intensity, and processed images may even have floating point (as opposed to integer) and negative values (e.g., images obtained through subtraction or logarithmic operation). Scaling operations permit rescaling of the input image for display or other purposes. Examples of scaling functions are illustrated in Table 2.

3.1.2 Contrast Transformation

Image contrast can be manipulated using image grey level dependent transformation f, so as to stretch or compress the contrast information within specified segments of the input image dynamic range. Examples of contrast transformation operators are given in Table 3.

The piecewise linear transformation is the most frequently-used mapping for stretching or compressing the contrast over selected segments of grey levels. The values of the segment slopes α, β, and γ determine whether the contrast in the regions $[0,a]$, $[a,b]$ and $[b,L]$ is stretched or shrunk. Thus, slopes less than 1 give rise to contrast compression; conversely, slopes greater than 1 result in contrast stretch. For example, $\alpha > 1$, $\beta < 1$ and $\gamma < 1$ results in a mapping that enhances the contrast in the dark regions $[0,a]$ of the input image and compresses the brighter portions $[a,L]$. The reverse effect may be obtained by setting $\alpha < 1$, $\beta > 1$ and $\gamma > 1$.

The logarithmic transformation expands the contrast of the dark regions of u (i.e., u small) and compresses the brighter intensity levels. Information content in the low contrast input image is improved by enhancing the low contrast edges. Furthermore, multiplicative noise is transformed into additive noise. Note that before applying the logarithmic transformation the input image grey levels must be constrained or mapped to values equal to or greater than 1.

Table 2. Examples of Scaling Functions

Scaling Function	Mapping v = f(u)
a). Linear Image Scaling with Thresholding	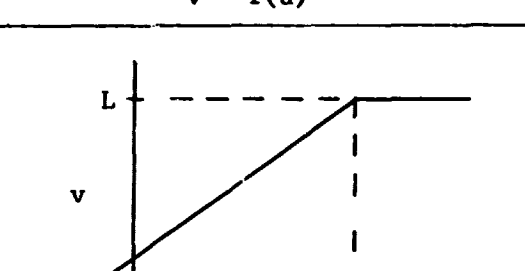
b). Reverse Scaling	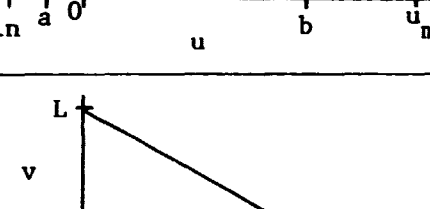
c). Grey Level Window Slicing (Without Background)	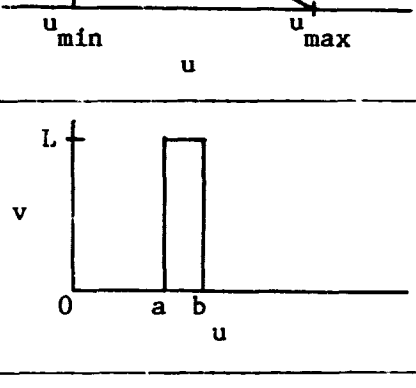
d). Grey Level Window Slicing (With Background)	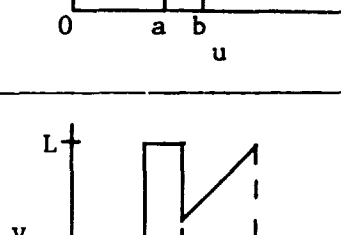

Table 3. Contrast Transformation Operators

Contrast Transformation	Maping v = f(u)
a). Piecewise Linear Transformation - 3 segment operator	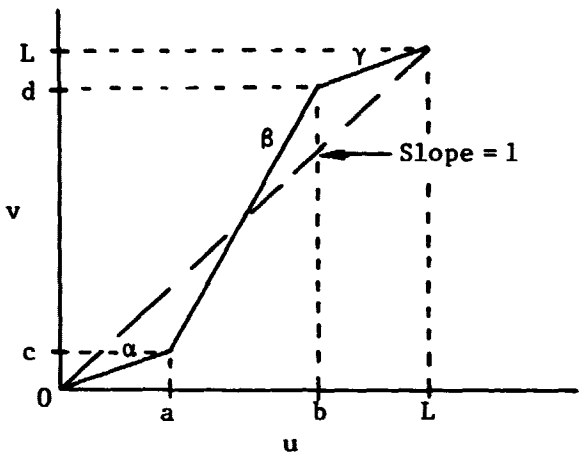
b). Logarithmic Transformation v = k log u	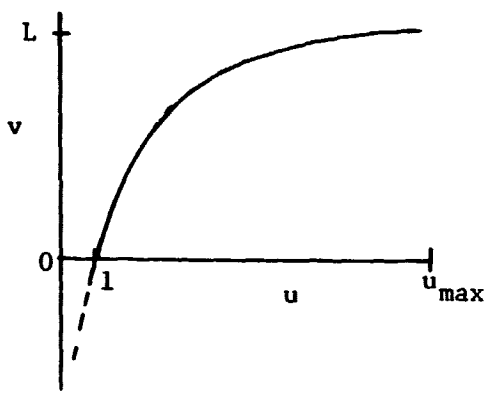
c). Exponential Transformation $v = k e^{u}$	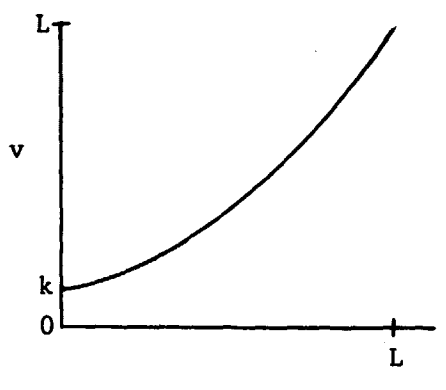

The exponential transformation is the inverse of the logarithmic operation; as a result, low intensity segments are compressed while higher intensity regions are expanded. This operation is not useful in most cases because the processed image has generally less visible detail than the original.

3.1.3 Histogram Equalization and Modification

Given a digital image $u(x,y)$ that is quantized into L grey levels q_0, q_1, ..., q_{L-1}, let $p_u(q_i)$ denote the relative frequency with which grey level q_i occurs in u, for all q_i from i=0 to L-1. Then the bar graph of $p_u(q_i)$ as a function of q_i, normalized so that

$$\sum_{i=0}^{L-1} p_u(q_i) = 1$$

is called the histogram of u. Histogram modification can be achieved by selecting an appropriate grey scale transformation v=f(u) such that the transformed image v has a specified histogram $p_v(r_k)$. When the specified output image histogram is $p_v(r_k)$= constant (i.e., uniform distribution), the process is called histogram equalization.

It can be shown that histogram equalization of an image u may be achieved using the grey level transformation.

$$r_k = F_u(q_k) = \sum_{i=0}^{k} p_u(q_i) \quad : k= 0,1,\ldots,L-1$$

Since the original grey level values q_i are integers, and the distribution function varies between 0 and 1, the grey level values r_k of the transformed image v must be scaled to L integer levels. This is accomplished by the scaling operation

$$v_k = \text{Int}\left[L\left(\frac{r_k - r_{min}}{r_{max} - r_{min}}\right) + 0.5 \right]$$

where Int is the integer truncation function and 0.5 is added to provide symmetrical rounding. Note that the effect of histogram equalization is to produce an image where all the grey levels occur equally often. The result is

an image that shows higher contrast over the entire range of grey levels. In other words, by creating an image with a flatter histogram than the original, the pixels in the densely-populated regions of the grey scale are assigned a larger grey scale region and vice-versa. This provides contrast enhancement by stretching of the high density grey level segments and a compression of the sparsely-populated segments.

Histogram modification may be obtained appropriately using the equalization procedure on the histogram of the original image, and the inverse equalization process on the specified histogram. Thus, an input image u with a histogram $p_u(u)$ may be transformed to an output image v with a specified histogram $p_v(v)$ by a three-step procedure as follows:

1. Histogram equalize the original image

$$s=f(u)$$

2. Specify the desired histogram function and obtain the equalizing transformation $g(v)$.

3. Apply the inverse transformation $v=g^{-1}(s)$ to the previously equalized image s.

These three steps can be combined into one operation on the original image u ; thus:

$$v = g^{-1}[f(u)]$$

The resulting output image v should have the specified histogram $p_v(v)$.

Histogram specification is useful in matching images obtained from various sensors (e.g., visual, infrared, radar, etc.) or for correlation of multiple scenes obtained under different environmental conditions.

3.2 Spatial Operations

Spatial operations involve the processing of a group of image pixels within a small neighborhood of a given pixel. Thus, each input image pixel u(m,n) is processed by considering its surrounding pixels over a finite window W to produce an enhanced image pixel v(m,n). Typical windows are as follows:

a) W_1 =

m \ n	0	1
0	•	•
1	•	•

: 2 x 2 window with origin at left upper corner

b) W_2 =

m \ n	-1	0	1
-1	0	•	0
0	•	•	•
1	0	•	0

: 5 point nearest neighbor window with origin at center

c) W_3 =

m \ n	-1	0	1
-1	•	•	•
0	•	•	•
1	•	•	•

: (3 x 3) window with origin at center

These windows are sequentially scanned over the input image (with the window origin centered on the input image pixel) to produce a processed output typically used for enhancing raw image data.

3.2.1 Spatial Averaging

Spatial averaging involves replacing each input pixel value by its local mean over a prescribed neighborhood or window. Thus, given an input image pixel u(m,n), the output value v(m,n) is given by the relation

$$v(m,n)=\bar{u}(m,n) = \frac{1}{N_W} \sum_{(k,\ell)\in W} u(k,\ell)$$

where W is the averaging window and N_W are the number of points in the window over which the local mean is computed. Windows typically used are shown below.

k \ ℓ	n	n+1
m	1	1
m+1	1	1

a) (2x2) : $N_W = 4$

k \ ℓ	n-1	n	n+1
m-1	1	1	1
m	1	1	1
m+1	1	1	1

b) (3x3) : $N_W = 9$

k \ ℓ	n-1	n	n+1
m-1	0	1	0
m	1	1	1
m+1	0	1	0

c) (3x3) : $N_W = 5$

The effect of spatial averaging is to increase the signal-to-noise ratio of the image by averaging out the noise. Spatial averaging works best for images that contain additive white noise. The noise reduction is achieved at the expense of blurring the signal through averaging. Larger windows increase the blurring of the image while reducing the noise, and vice versa. A suitable window size must be determined to fit the requirements of a given image.

Thus, given an input image

$$u(m,n) = s(m,n) + \eta\,(m,n)$$

consisting of signal s and zero mean white noise η with power σ_η^2 the spatial averaged output image

$$v(m,n) = \bar{u}\,(m,n)$$
$$= \bar{s}\,(m,n) + \bar{\eta}\,(m,n)$$

where $\bar{\eta}$ is the averaged noise over window W with zero mean and power

$$\sigma_{\bar{\eta}}^2 = \frac{1}{N_W}\,\sigma_\eta^2$$

and signal $\bar{s}$ that is a smoothed or blurred version of the original signal s over the window W. Thus, the image signal-to-noise ratio is improved by an integer factor of N_W.

Since spatial averaging achieves noise reduction at the expense of creating a blurred image, an alternative approach is to use a directional smoothing algorithm. This is a nonlinear filter that preserves the line edges and boundaries while smoothing out additive noise. This is achieved by replacing a pixel value by its local average along a direction of minimum gradient. Thus, the output image

$$v(m,n) = \bar{u}(m,n,\theta^*) = \frac{1}{N_W} \sum_{(k,\ell)\,\varepsilon C_{\theta^*}} u(k,\ell)$$

where C_{θ^*} shown in Figure 7 is a window with N_W points, centered at (m,n) with pixels along a minimum gradient direction θ^*.

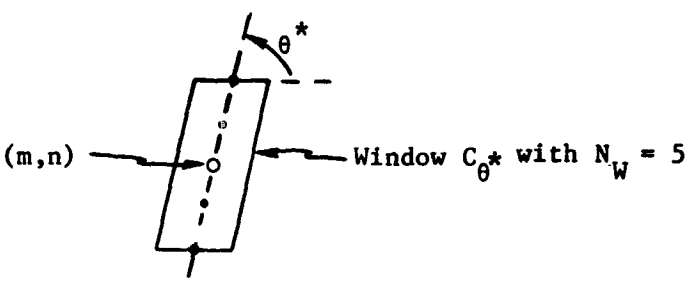

Figure 7: Window C_{θ^*} along direction θ^*.

Here $\bar{u}(m,n,\theta) = \frac{1}{N_W} \sum_{(k,\ell)\varepsilon C_\theta} u(k,\ell)$

$\Delta(\theta) = |\, u(m,n) - \bar{u}(m,n,\theta)\,|$

and $\theta^* = \min_{\theta} \{\Delta(\theta)\}$

3.2.2 Median Filtering

Median filtering is a nonlinear spatial processing algorithm where each pixel value is replaced by its local median value over a prescribed neighborhood or window W. Thus, given an input image u(m,n), the median filtered image v(m,n) is given by the nonlinear operation.

$$v(m,n) = \text{median}\ \{u(k,\ell):(k,\ell)\ \varepsilon\ W \text{ centered on } (m,n)\}$$

By necessity, the number of points, N_W, in the window W must be odd. To illustrate the concept, let

$$u(m) = [1\ \ 2\ \ 3\ \ 8,\ 4,\ 3,\ 2,\ 1]$$

be a one-dimensional sequence of pixel values. Then, median filtering with a 3-pixel sliding window with the input image pixel m at the center, results in an output pixel sequence v(m) as shown in Figure 8.

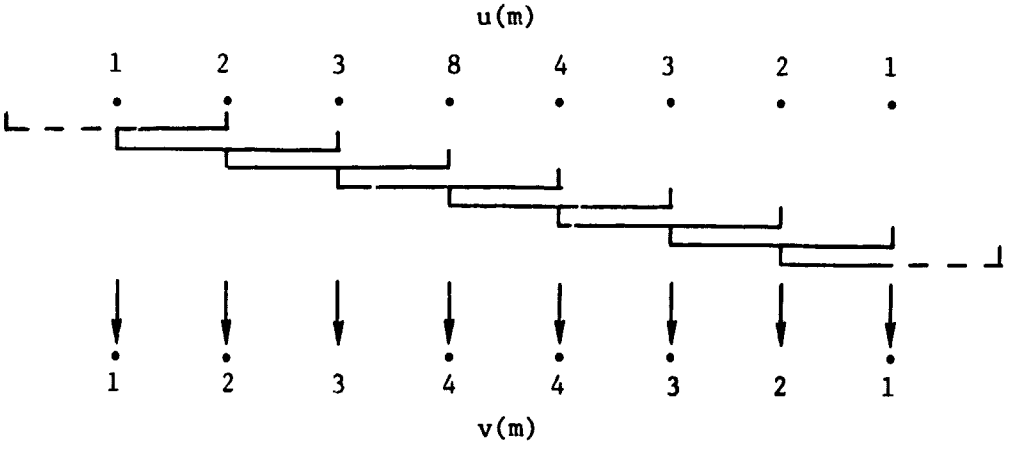

Figure 8. (1x3) Window Median Filtering

The median filtering algorithm consists of the following steps: 1) choose a window W with an odd number (N_W) of pixels, (2) center the window W on the input image pixel under consideration, (3) arrange the input image pixel values in the window W in a non-decreasing order, (4) pick the center value, (5) choose the center value computed in step 4 as the cutput value of the image pixel under consideration, and (6) slide the window W to the next pixel value and repeat steps 1 through 5. However, a straightforward implementation of this algorithm is computationally slow. Huang, et al. [6] have derived a recursive algorithm that is computationally far superior than the one described above which involves sorting.

The median filter is most useful for removing isolated or binary noise in the form of lines or points without resulting in any loss in spatial resolution. Noise pixels are suppressed as long as their number in a window is less than $\frac{1}{2} N_W$. The median filter, unlike spatial averaging, does not suppress Gaussian wide band noise.

3.2.3 Spatial High Pass Filtering

A spatial high pass filter is the complement of a spatial low pass filter or averaging operation. Thus, the output of a high pass filter is given as

$$v(m,n) = [1 - \text{Low Pass Filter}].\ u(m,n)$$
$$= u(m,n) - \{ u(m,n)\}_{\text{Low Pass}}$$

where $\{u(m,n)\}_{\text{Low Pass}} = \bar{u}(m,n)$

is the output of a spatial averaging filter as described in Section 3.2.1. The effect of spatial high pass filtering is to enhance the high frequency spatial characteristics (i.e., lines, edges, etc.) of input images.

3.2.4 Unsharp Masking

Unsharp masking is a method of accentuating the edges in an image to provide a subjectively pleasing look to the enhanced image. The basic idea is to add varying amounts of the edge features extracted using a high pass filter to the original image to produce an image with crispened edges. The steps involved are illustrated in Figure 9.

In this figure, the abscissa is the direction r of the image intensity gradient (from black to white), and the ordinate is the image grey level intensity. The high pass filtered image is obtained by applying a high pass spatial filter to the original image (a) or by subtracting the low pass filtered image (b) from the original image (a). Adding this high pass image (c) to the original image (a) gives the unsharp masked image (d) with enhanced edge features.

3.2.5 Statistical Scaling

The purpose of statistical scaling is to provide uniformity in the dynamic range of image pixels. This is achieved by normalizing each pixel value with respect to its local standard deviation as follows.

$$v(m,n) = \frac{u(m,n)}{\sigma_{m,n}}$$

where $$\sigma_{m,n} = \left\{ \frac{1}{N_W} \sum_{(k,\ell)\,\varepsilon\, W_{m,n}} \left[u(k,\ell) - \mu_{m,n} \right]^2 \right\}^{1/2}$$

is the standard deviation of the image in a finite N_W point window $W_{m,n}$ centered at the given pixel (m,n), and

$$\mu_{m,n} = \frac{1}{N_W} \sum_{(k,\ell)\,\varepsilon\, W_{m,n}} u(k,\ell)$$

is the local mean over the same window $W_{m,n}$. The effect of this operation is to enhance the pixels whose grey level intensity is noticeably larger than the

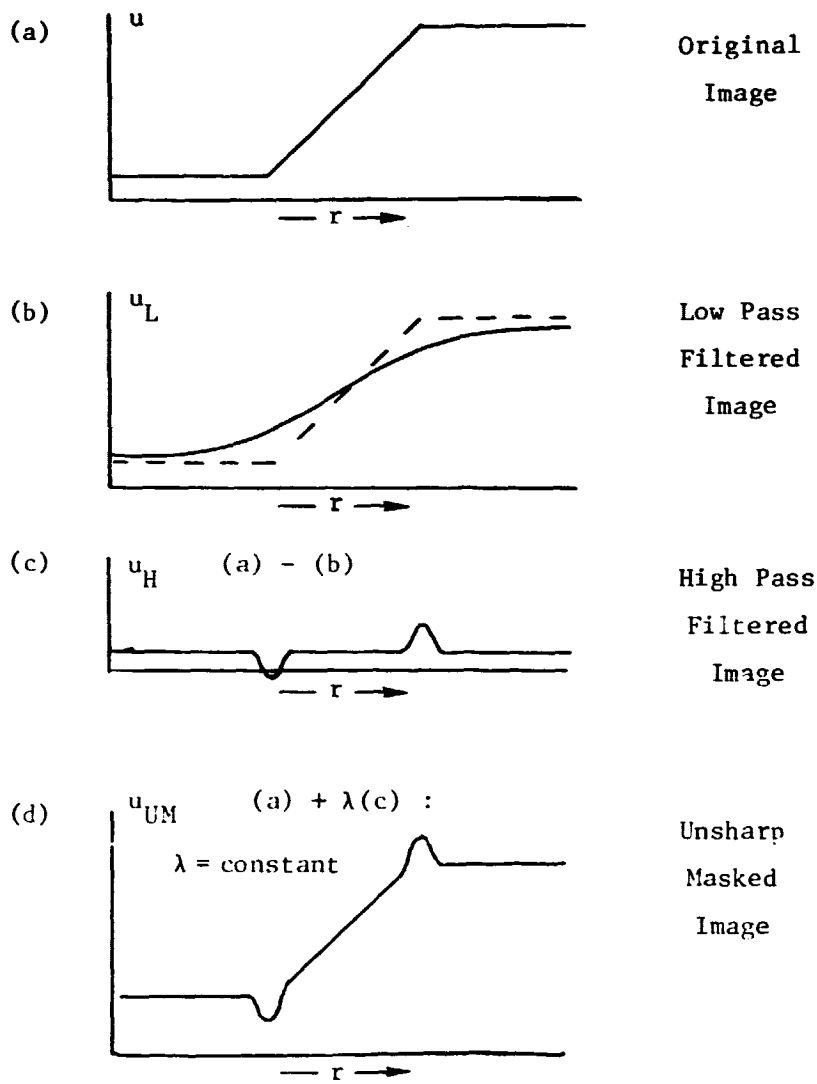

Figure 9. Unsharp Masking Procedures

surrounding average value. The result is the enhancement of edge features in the original image. It should be noted, however, that this algorithm can also indiscriminately enhance impulse noise present in a raw image.

There are many other enhancement techniques such as pseudocoloring, various special masks for high pass filtering, interpolation and super-resolution (using the point-spread function of the imaging device for deconvolution) that are described in the literature. Greater details on these and other methods may be found in the standard references [1-5].

3.3 Edge Detection Operations

Edge detection implies the determination of the boundary of natural or man-made features in a given image. Such an edge enhanced image can be used to identify man-made objects such as buildings, railway tracks, helicopters, ground vehicles and highways. In airborne radar navigation and guidance, edge detection algorithms, followed by edge thinning, could be useful to present clear and uncluttered images of the terrain and target features. A large number of edge detection algorithms have been devised with varying degrees of success. The basic form of the algorithm is to convolve the given image with a finite two-dimensional matrix operator and threshold the result to extract edge, gradient, or line boundaries. Thus, given an input image $u(m,n)$, and a matrix operator $h(m,n)$, then the edge-enhanced image $v(i,j)$ is given by the convolution

$$v(i,j) = \langle U,H \rangle_{i,j} = \sum_{m} \sum_{n} h(m,n)\, u(i+m,\, j+n)$$

An edge map of this image may be obtained by thresholding the edge-enhanced image $v(i,j)$ at some value K_T.

There are a number of different edge enhancement algorithms that may be utilized for edge detection. Many of them are identified by the name of the investigator who was associated with its development. However, a closer look at these methods shows that they may be classified into two broad categories--directional linear gradient operators and nonlinear average gradient detection algorithms.

3.3.1 Directional Gradient Operators

Directional gradients, or the so-called compass gradients, may be obtained using two dimensional discrete differentiation. Table 4 shows four different directional gradients which are useful in detecting North going edges. An anti-clockwise circular shift of the eight boundary elements of any of these masks gives a 45^{o} rotation of the compass gradient operator.

Table 4. Four North Directional Gradient Operators

Compass: $\begin{bmatrix} 1 & 1 & 1 \\ 1 & -2 & 1 \\ -1 & -1 & -1 \end{bmatrix}$	Robinson: $\begin{bmatrix} 1 & 1 & 1 \\ 0 & 0 & 0 \\ -1 & -1 & -1 \end{bmatrix}$
Kirsch: $\begin{bmatrix} 5 & 5 & 5 \\ -3 & 0 & -3 \\ -3 & -3 & -3 \end{bmatrix}$	Robinson: $\begin{bmatrix} 1 & 2 & 1 \\ 0 & 0 & 0 \\ -1 & -2 & -1 \end{bmatrix}$

Thus, for example, the operator

$$\underline{H} = \begin{bmatrix} 1 & 1 & 1 \\ 1 & -2 & -1 \\ 1 & -1 & -1 \end{bmatrix}$$

would be a NW compass gradient operator. In this manner eight compass gradients can be defined. Letting $g_{\theta}(m,n)$ denote the compass gradient in direction θ with

$$\theta = \frac{\pi}{2} + \frac{K\pi}{4} \quad , \quad K = 0,\ldots,7$$

$$\text{let } g_{max}(m,n) = \max_{\theta} \{g_{\theta}(m,n)\} \tag{2}$$

then $g_{max}(m,n)$ is compared against a threshold to detect an edge. Figure 10 describes these operations in a block diagram form.

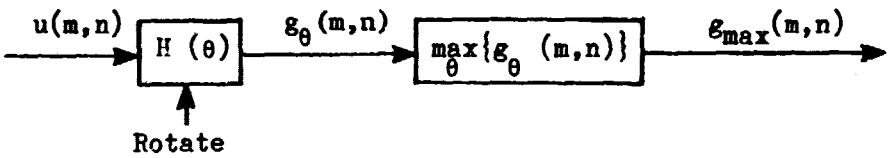

Figure 10. Compass Gradient-Processing

3.3.2 Average Gradient Detection Operators

A two-dimensional edge is said to exist in an image whenever the luminance changes considerably within a few pixels. Figure 11 shows a generic block diagram describing the computation of the average gradient detection operators. Table 5 shows some of the edge detection operators. The masks H_1

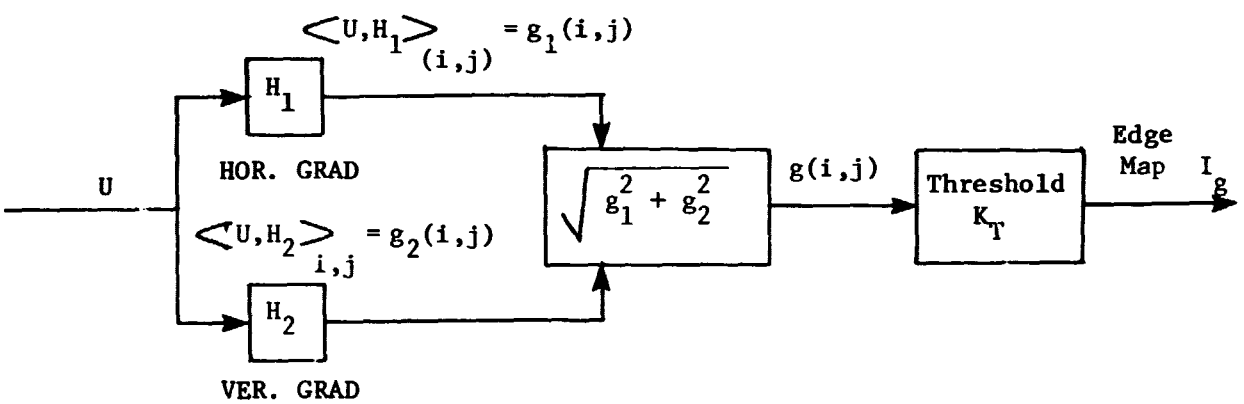

Figure 11. Average Gradient Detection Algorithm

and H_2 are used to compute the gradients g_1 and g_2 in the horizontal and vertical directions. Then the average gradient is given as

$$g(i,j) = \sqrt{g_1^2 + g_2^2}$$

where $g_1 = \langle U, H_1 \rangle_{(i,j)}$

$g_2 = \langle U, H_2 \rangle_{(i,j)}$

and $\langle U,H \rangle_{(i,j)} \triangleq \sum_m \sum_n h(m,n)u(i+m,j+n)$

where $h(m,n)$ are the elements in the masks given in Table 5. Finally, the edge map is obtained by thresholding the average gradient image $g(i,j)$ and is defined as the set of edge points given by

$$I_g = \{(i,j) : g(i,j) > K_T\}$$

Table 5. Some Common Edge Detection Operators

Edge Detection Operators	H_1	H_2
1. Robert's Gradient	$\begin{bmatrix} 1 & 0 \\ 0 & -1 \end{bmatrix}$	$\begin{bmatrix} 0 & 1 \\ -1 & 0 \end{bmatrix}$
2. Smoothed Gradient	$\begin{bmatrix} 1 & 1 & 1 \\ 0 & 0 & 0 \\ -1 & -1 & -1 \end{bmatrix}$	$\begin{bmatrix} 1 & 0 & -1 \\ 1 & 0 & -1 \\ 1 & 0 & -1 \end{bmatrix}$
3. Sobel Operator	$\begin{bmatrix} 1 & 2 & 1 \\ 0 & 0 & 0 \\ -1 & -2 & -1 \end{bmatrix}$	$\begin{bmatrix} 1 & 0 & -1 \\ 2 & 0 & -2 \\ 1 & 0 & -1 \end{bmatrix}$
4. Isotopic Gradient	$\begin{bmatrix} 1 & \sqrt{2} & 1 \\ 0 & 0 & 0 \\ -1 & -\sqrt{2} & -1 \end{bmatrix}$	$\begin{bmatrix} 1 & 0 & -1 \\ \sqrt{2} & 0 & -\sqrt{2} \\ 1 & 0 & -1 \end{bmatrix}$

Another common approach to edge enhancement that does not depend upon edge direction is based on the use of Laplacian masks. These operators shown in Table 6 represent discrete approximations of the continuous Laplacian differential operator

$$L = \frac{\partial^2}{\partial x^2} + \frac{\partial^2}{\partial y^2}$$

and are indicative of the sum of second derivatives in two orthogonal directions (e.g., horizontal/vertical or two diagonals). These operators are very sensitive to noise in the data.

Table 6. Discrete Laplacian Operators

1) $\begin{bmatrix} 0 & -1 & 0 \\ -1 & 4 & -1 \\ 0 & -1 & 0 \end{bmatrix}$	2) $\begin{bmatrix} -1 & -1 & -1 \\ -1 & 8 & -1 \\ -1 & -1 & -1 \end{bmatrix}$
3) $\begin{bmatrix} 1 & -2 & 1 \\ -2 & 4 & -2 \\ 1 & -2 & 1 \end{bmatrix}$	4) $\begin{bmatrix} 1 & 0 & 1 \\ 0 & -4 & 0 \\ 1 & 0 & 1 \end{bmatrix}$

In Table 6, for example, mask (1) represents the difference of the first differences along the middle horizontal and vertical directions. In mask (2), this operation is done over the four directions (horizontal, vertical and 2 diagonal) passing through the center of the mask. Similar explanations may be given for masks (3) and (4) in Table 6.

4. OVERWATER RADAR IMAGE ENHANCEMENT

The overwater scenario shown earlier in Figure 1 consists of an oil rig and a tugboat in the Gulf of Mexico, off the coast of Louisiana. A plan view sketch of this oil rig is shown in Figure 12. An example of the sum(s) radar image for this scenario is as shown in Figure 5. Notice that this sum radar image consists of two recognizable pixel clusters (the left cluster being slightly below the right) corresponding to the two platforms, joined together by an almost continuous diagonal row of visible pixels representing the connecting catwalk. Adjacent to the left platform is a small group of pixels that correspond to the tugboat shown in the photograph of Figure 1. The radar image of Figure 5 shows that the two oil rig platform clusters cover a relatively small area (approximately 36 x 36 pixels per cluster) compared to the overall (412 x 286) pixel image. As a result, the information contained in this scene that is pertinent to the pilot's flying task is restricted to only a very small region of the overall radar image.

Because of the peculiar nature of this image scenario, the objective of image enhancement is to present to the pilot a processed image that shows the image features that are pertinent to the actual oil rig shown in Figure 1; namely, the location of the two platforms, the connecting catwalk, the left and right towers (50 m and 70 m, respectively) and the left and right helipads (12 x 15 sq.m each). Unfortunately, since each of the helipads only cover a small number of pixels (5 in range and 10 in azimuth) in the radar image of Figure 5, it is not likely that their location can be identified strictly through application of image enchancement techniques alone. The only hope is the possibility that a strong radar signature exists which uniquely characterizes the helipads and hence can be used for extracting the image pixels corresponding to their location.

Before proceeding with the task of radar image enchancement, it is necessary to analyze the statistical characteristics of the image data. The following section describes the results of image data analysis.

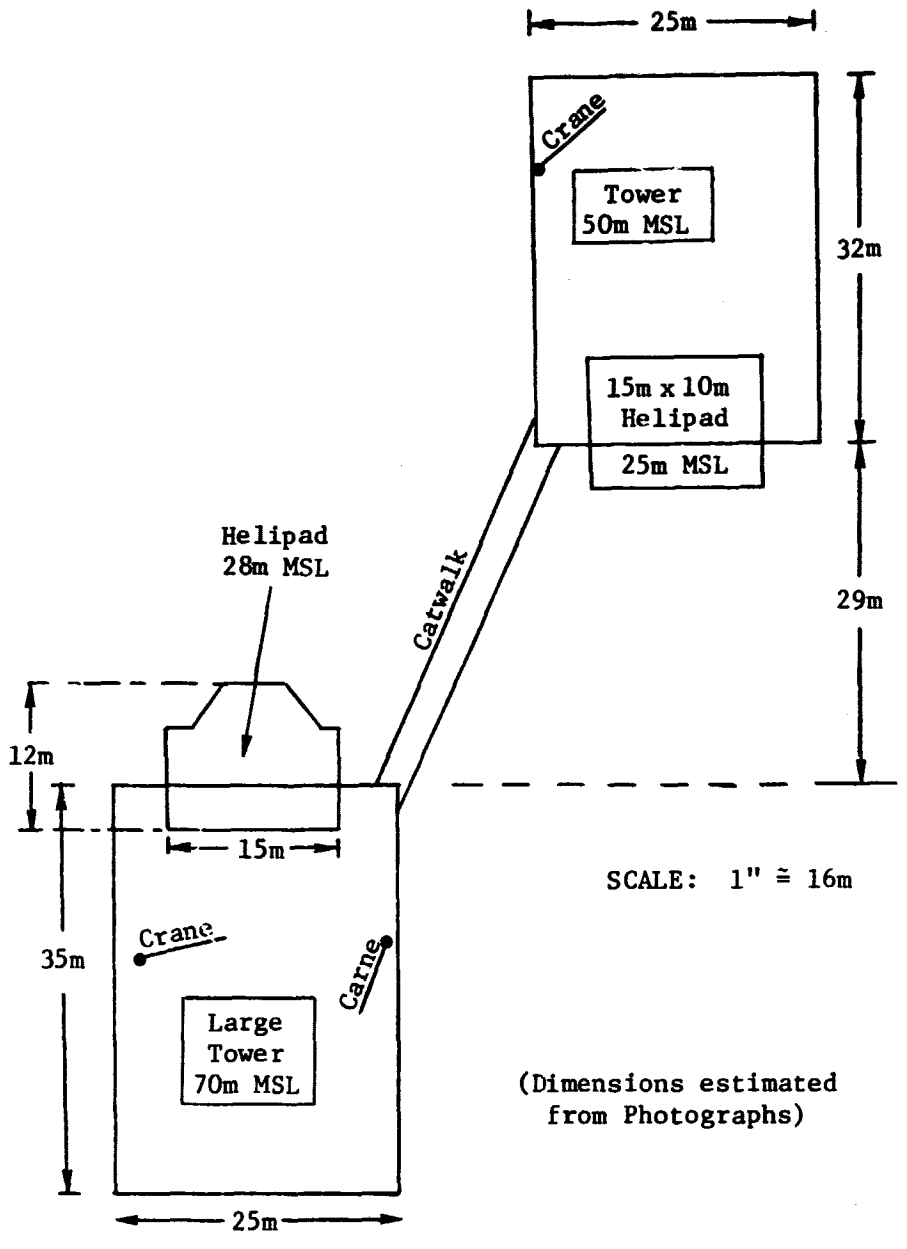

Figure 12. Plan View Sketch of Oil Rig

4.1 Characteristics of Overwater Radar Images

Even (E) and odd (O) overwater radar image data was processed to determine the statistical charactertistics of the image segments corresponding to the ocean clutter, the platform target and the connecting catwalk. Histograms for the ocean, platform target and catwalk regions are shown in Figures 13-15. In addition, Figure 16 shows a histogram for the sum normalized even and odd images, respectively. These histograms assume that the individual pixel values in each of these three regions are generated from corresponding but distinct homogeneous distributions. In other words, knowledge about any existing variations in pixel values by spatial location is not taken into consideration. Additional plots of the spatial distibution of pixels corresponding to various combinations of even and odd image pixel value ranges (e.g., high even and high odd, high even and low odd, low even and high odd, low even and low odd) were made to determine if pixel cluster patterns exist corresponding to known physical features of the oil rig (e.g., towers, catwalk, helipads, and platform boundaries). Based upon the analysis of these data, the following observations are pertinent.

1. Even and odd ocean clutter have almost identical Gaussian distributions: $N(\mu \cong 22, \sigma \cong 7)$

2. Even and odd platform target distributions are Gaussian and distinguishable: $N_E(\mu \cong 105, \sigma \cong 33)$, $N_O(\mu \cong 68, \sigma \cong 30)$

3. Even and odd catwalk distribution are similar for pixel values less than 50. However, the even catwalk image has significant number of pixels with grey levels greater than 50.

4. a. High even and high odd pixel values correspond to location of tall structures (e.g., the two towers)

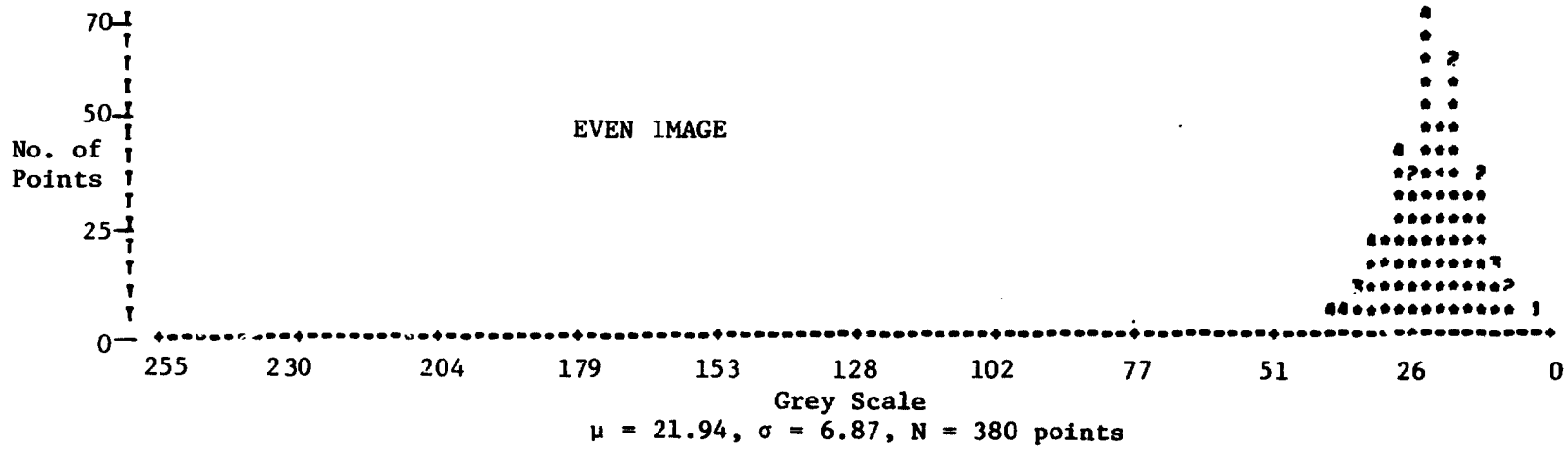

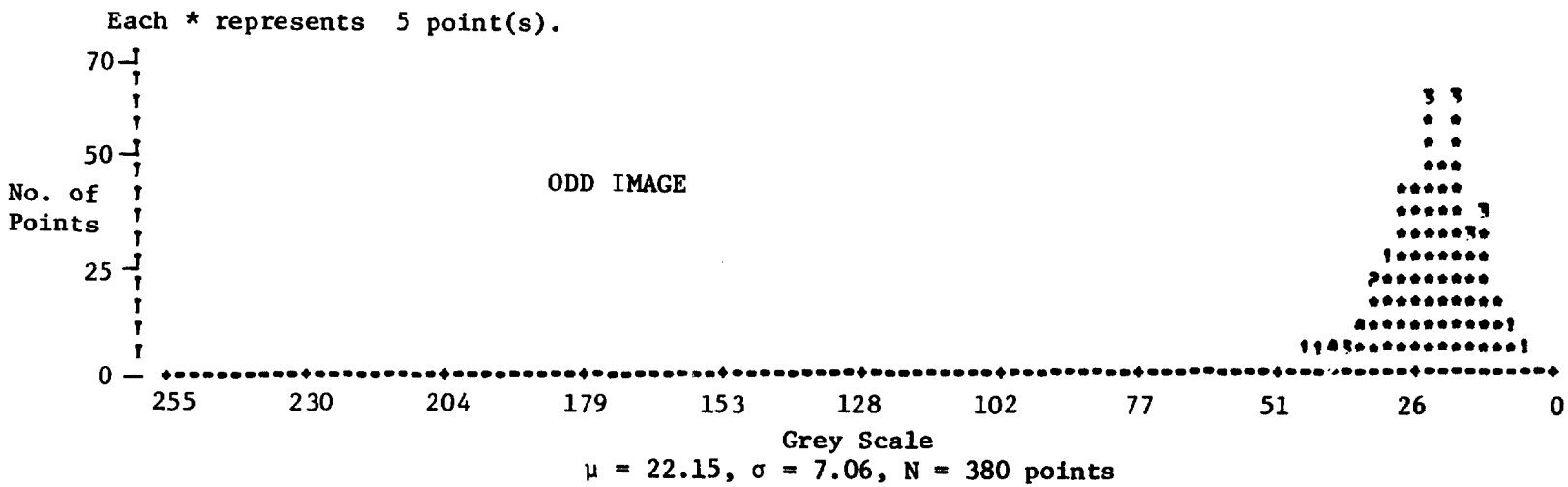

Figure 13. Ocean Clutter Histograms

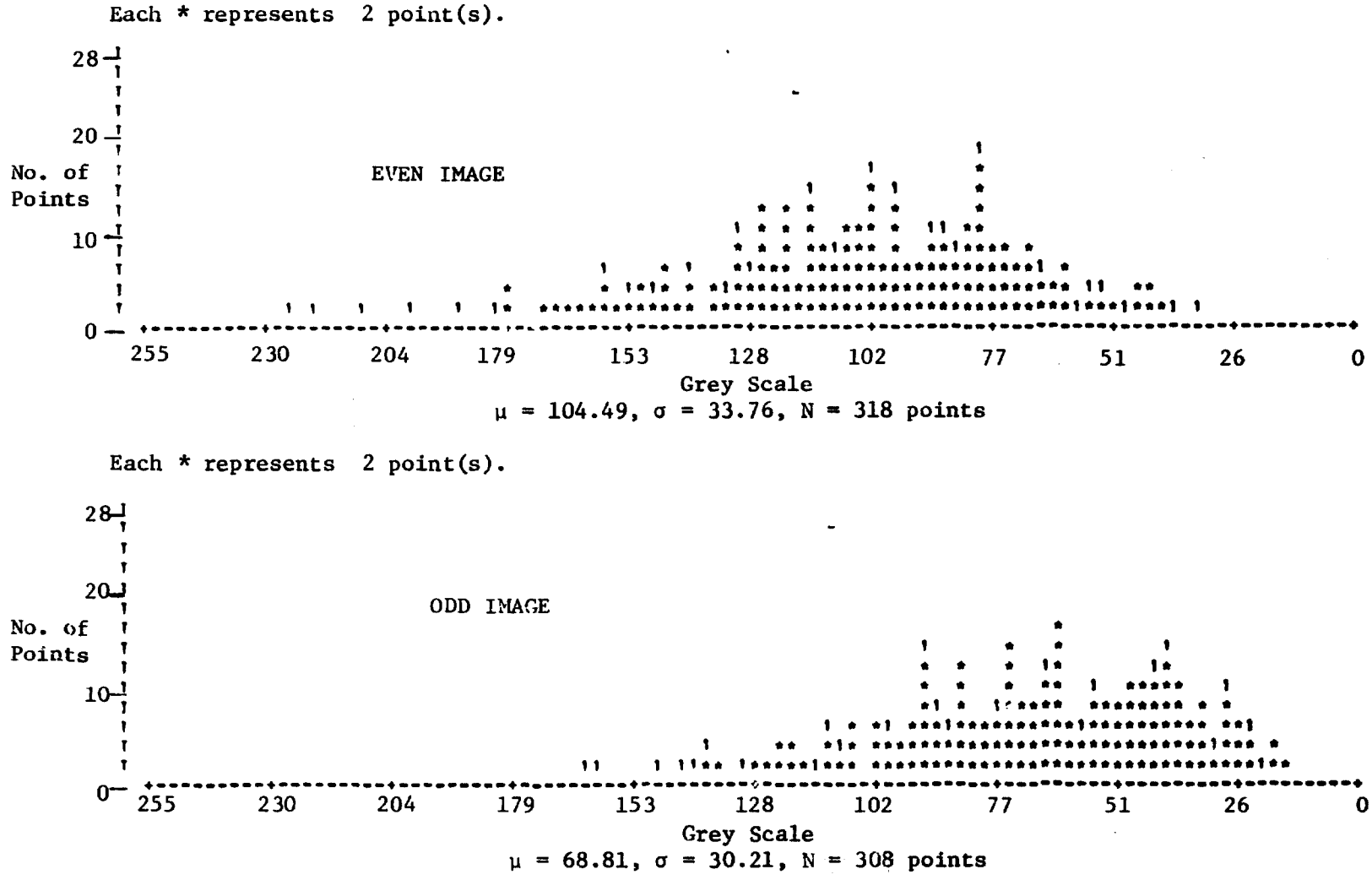

Figure 14. Platform Target Histograms

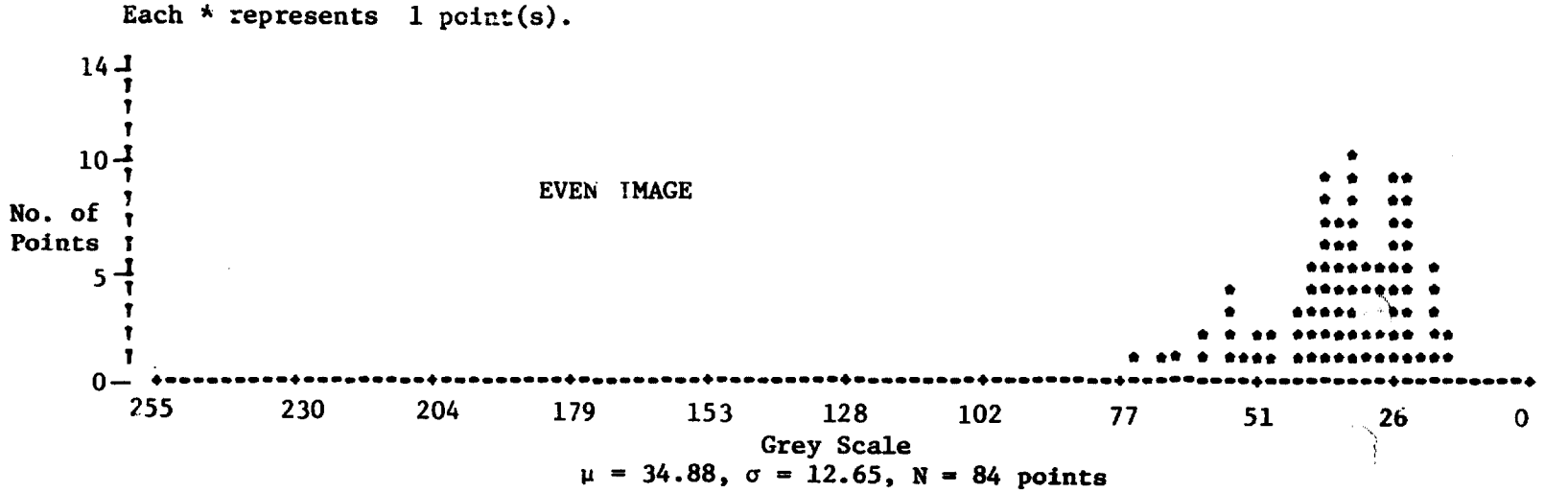

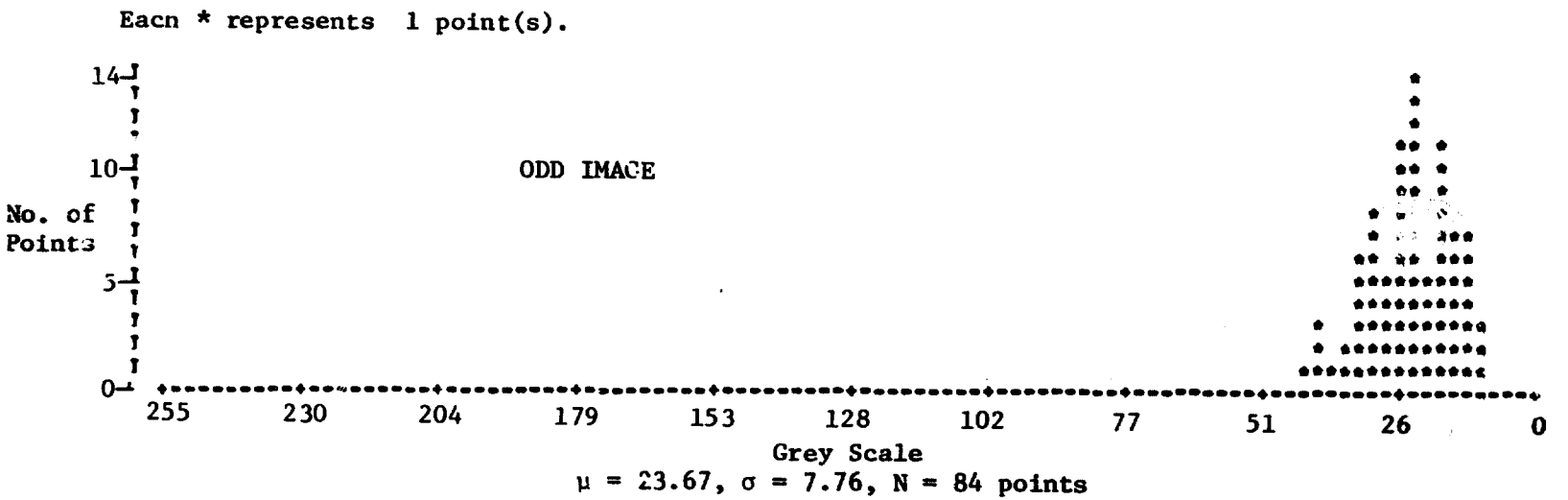

Figure 15. Catwalk Histograms

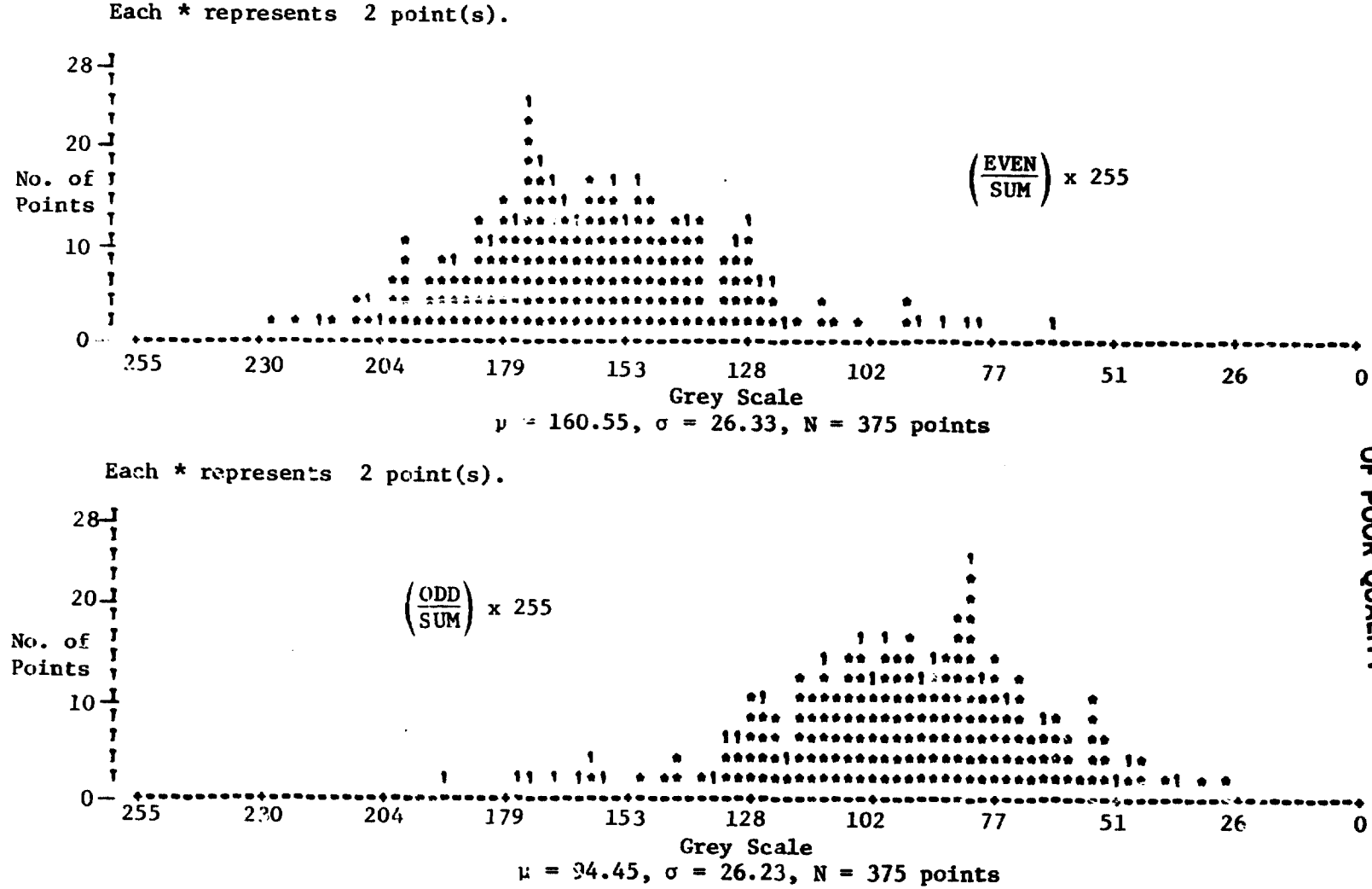

Figure 16. Sum Normalized Platform Target Histograms

b. High even and low odd pixel values correspond to pixels located at the top edge (i.e., longer range returns) of platform target image.

c. Low even and high odd pixel values correspond to pixels located at the bottom edge (i.e., shorter range returns) of platform target image.

d. Low even and odd pixel values correspond to ocean clutter pixel locations.

5. Histograms of normalized even and odd images show a greater separation in their mean values: N_{EN} ($\mu \approx 160, \sigma \approx 26$), N_{ON}($\mu \approx 94, \sigma \approx 26$). However, this increased separation does not provide any additional information that is not contained in the unnormalized images.

4.2 Overwater Image Enhancement

Amongst the observations made above, the items 4(b)-4(d) do not provide any useful information for detecting the helipads or any other meaningful features in the platform target image. However, the other observations provide information that is useful for image enhancement. Thus, items (1)-(3) based upon Figure 13-15 show that the target and clutter histograms are sufficiently nonoverlapping to allow removal of ocean clutter from the radar images by thresholding the even and odd images at a pixel value of 50. The threshold operator maps an input image u(m,n) into an output image v(m,n) by using the transformation

$$v(m,n) = \begin{cases} u(m,n) & : u(m,n) > K_T \\ 0 & : u(m,n) \leq K_T \end{cases}$$

where K_T is the value of the selected threshold grey level.

Improvements in the overwater radar image that can be obtained through thresholding and pseudocolor enhancement are shown in Figure 17-21. Thus, Figures 17 and 18 show the even and odd images prior to enhancement (Note that Figure 5 included earlier shows the sum image). Unfortunately, these original image photographs are not accurate copies of what can be viewed on a high resolution image display monitor. This is because of the peculiar nonlinear sensitivity of the photographic film. As a result, the catwalk, which is clearly recognizable on the displayed even image is not visible in the photographic print of Figure 17. However, significant improvement in the quality of the images can be obtained using thresholding with pseudocolor enchancement. Figures 19-21 show the even, odd and sum images after thresholding and pseudocolor processing. The pseudocolor mapping given in Table 7 was used to color the grey images of Figure 17, 18 and 5, respectively.

Table 7. Pseudocolor Mapping

Pixel Values	Color
[0 - 50]	Dark Blue
[51 - 100]	Light Green
[101 - 150]	Dark Green
[151 - 255]	Red

The range of pixel values [0-50] correspond to the ocean clutter and are therefore given the color dark blue. The color red is for pixel values greater than 150 and indicates the presence of high returns corresponding to the presence of tall structures (e.g., the two towers).

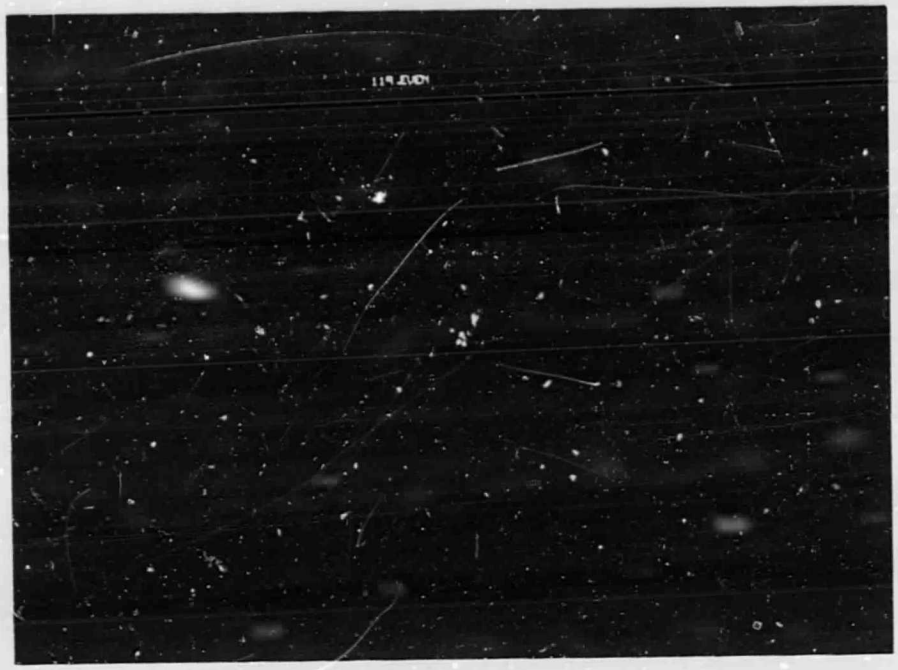

Figure 17. Overwater Even Radar Image

Figure 18. Overwater Odd Radar Image

Figure 19. Pseudocolor Enhanced Overwater Even Radar Image

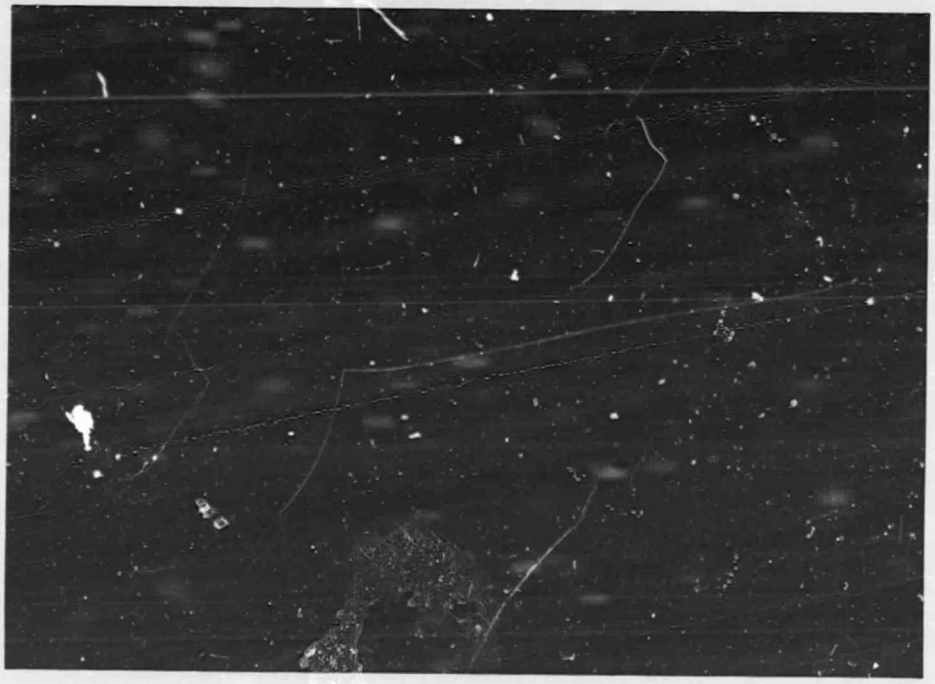

Figure 20. Pseudocolor Enhanced Overwater Odd Radar Image

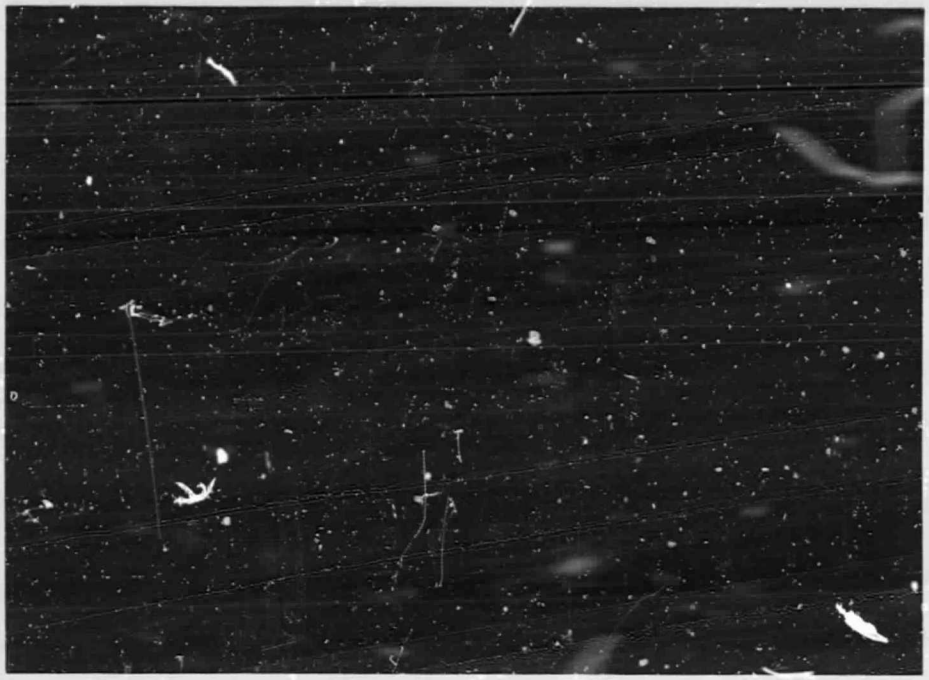

Figure 21. Pseudocolor Enhanced Overwater Sum Radar Image

Further improvements in the radar images may be obtained by producing an enhanced image that shows the two tower locations embedded in a target boundary image. The process of target boundary extraction (i.e., outline of the two platforms connected by a catwalk) involves the application of four image enhancement operators in sequence to the even image u_E as shown in the block diagram of Figure 22. As the first step, the raw even radar image is binarized using the operator

$$v_B(m,n) = \begin{cases} 0 \text{ (Black)} : u_E(m,n) < 50 \\ 255 \text{ (Red)} : u_E(m,n) > 50 \end{cases}$$

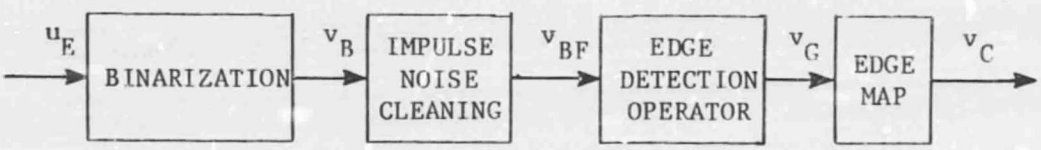

Figure 22. Target Boundary Extraction

The resulting binary image v_B is shown in Figure 23. Notice that the binary image v_B contains a substantial number of isolated or impulse noise pixels of high entensity (i.e., red). Impulse noise can be removed without blurring the rest of the image by median filtering the binary image. Figure 24 shows the results of applying a (1 x 3) median filter to the binary image v_B. The filtered image v_{BF} is almost clear of any impulse noise pixels. Finally, the target boundary or countour image in Figure 25 is extracted by processing the median filtered binary image v_{BF} with a Sobel gradient operator followed by an edge map (with a threshold of 30) or contour thinning operator. This image clearly shows the two platforms, the connecting sidewalk and a tugboat at bottom left.

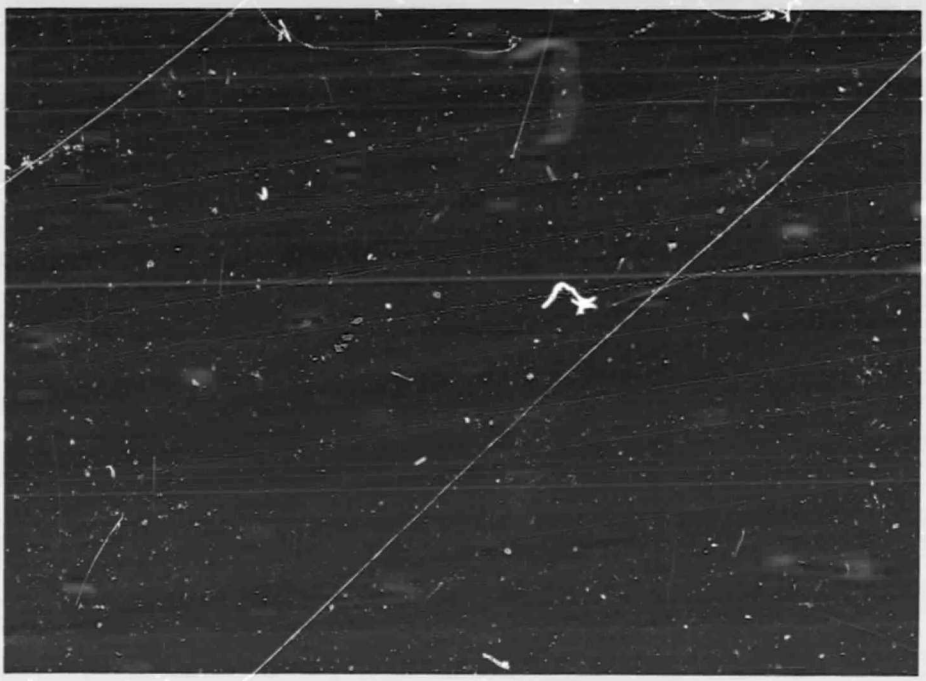

Figure 23. Binarized Platform Target Image v_B

Figure 24. Median Filtered Binary Platform Target Image v_{BF}

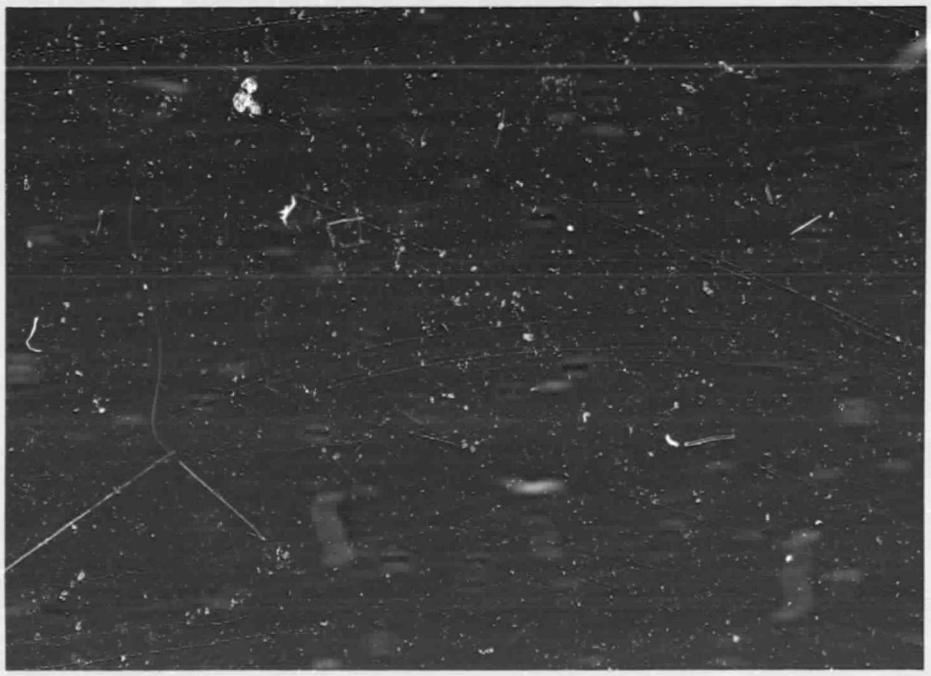

Figure 25. Target Boundary Image v_c

The tower locations are identified by using the observation that high pixel values for both even and odd images reflect the presence of tall structures. Thus, Figure 26 shows the algorithm used for the extraction of the tower locations. The procedure involves, as a first step, the binarization of the even and odd images using thresholds of K_E = 150 and K_O = 128, respectively. These thresholds were chosen (using the histograms in Figure 14) to isolate only the highest intensity pixels in the two images. The resulting two images v_{EH} and v_{OH} are further processed through a fuzzy AND operator to produce an image v_T that aggregates the high intensity pixel regions with the most overlap. The pixel locations extracted through this process are assumed to represent the tower locations in the radar image. Finally, Figure 27 shows the enhanced radar image v_P obtained by inserting the tower locations v_T extracted in Figure 26 into the target contour image v_c of Figure 25.

In order to check the validity of these aglorithms, two images (117 and 115) preceding the given image (119) were processed similarly to determine if the results were consistent. Figure 28 and 29 show the processed images v_P for the two cases. An examination of these three processed images (119, 117 and 115) in Figures 27-29 shows that both the tower locations and the surrounding boundary images shift through a consistent number of columns and rows from one image to another. This observation lends confidence to believing the high intensity pixel locations identified by the algorithm of Figure 26 as the tower locations.

4.3 Feasibility of Processing in Real-Time

The steps involved in processing the raw radar overwater images are: (1) thresholding, (2) binarization, (3) median filtering, (4) edge detection and (5) feature extraction. This section considers the basic arithmetic and logical operations involved in each of the processing steps. Assuming instruction cycle times for an Intel 8086 microprocessor running at a 10MHz clock frequency, processing times of each of the five steps/pixel are derived.

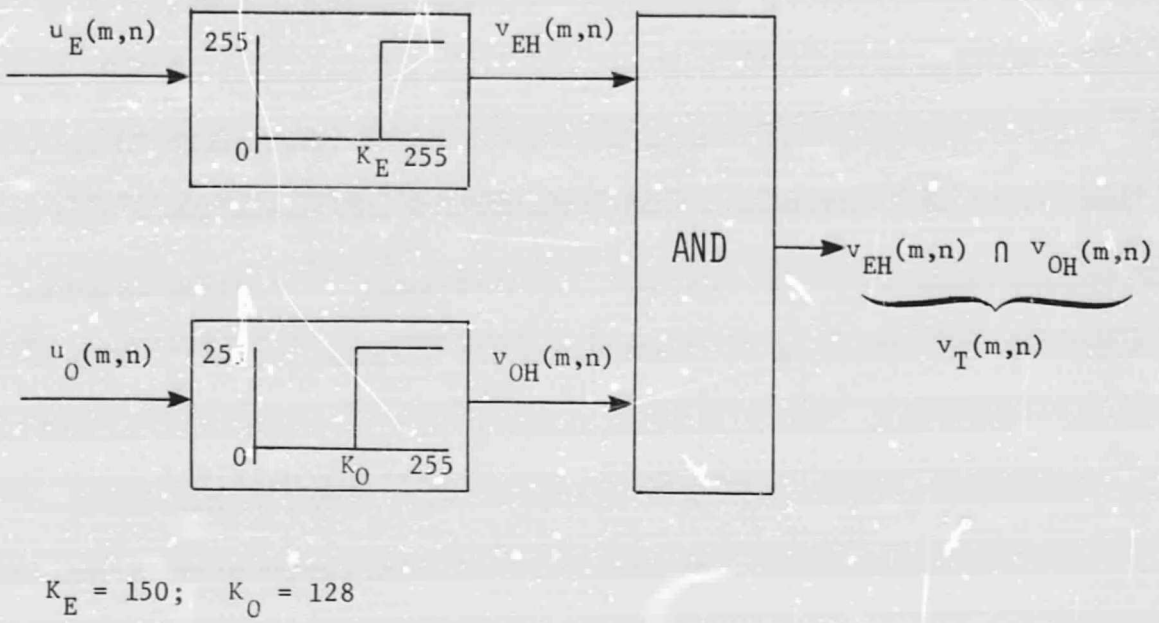

$K_E = 150$; $K_O = 128$

Figure 26. Tower Location Extraction Operator

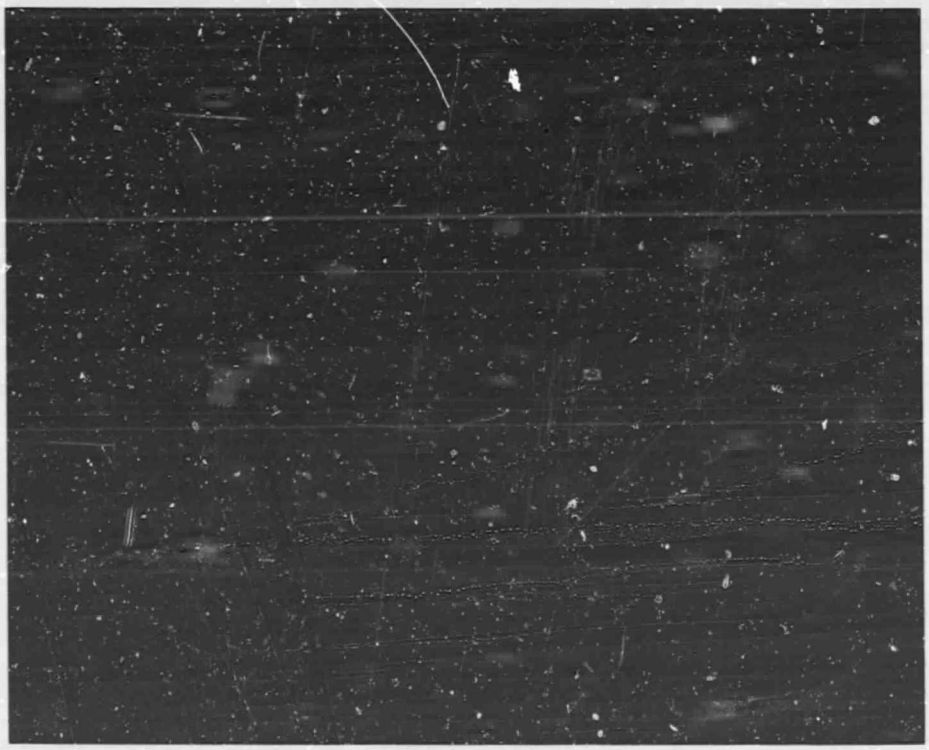

Figure 27. Enhanced Overwater Radar Image v_p (Image #119)

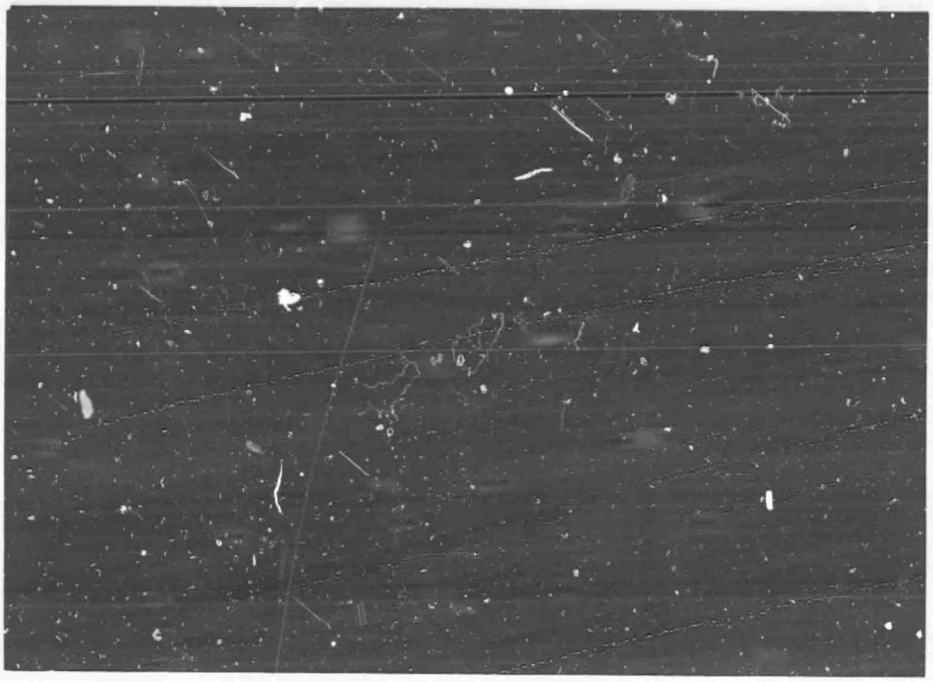

Figure 28. Enhanced Overwater Radar Image v_p (Image #117)

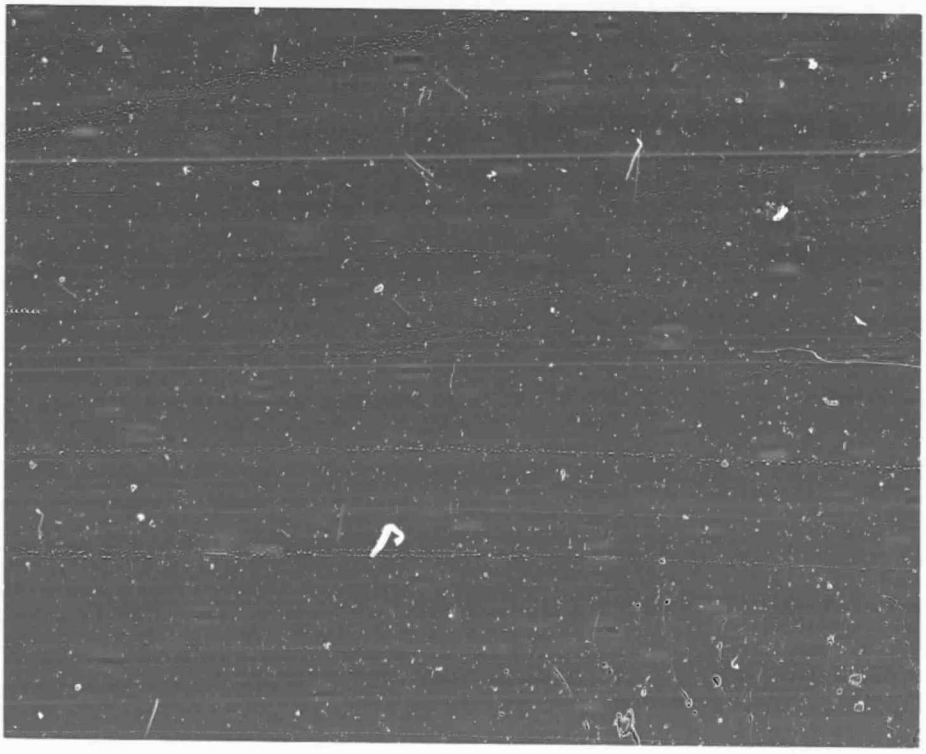

Figure 29. Enhanced Overwater Radar Image v_p (Image #115)

Thresholding. This step involves a conditional jump followed by a memory store. The processing time would be approximately 2 μs.

Binarization. This processing step is very similar to thresholding and would take the same processing time.

Median Filtering. The recursive algorithm consists of deleting n elements from a histogram and adding n elements as the nxn window is moved. The recursive computation of the median in the window involves basically comparing the previous median with the new pixels added. The total median filtering time/pixel is estimated to be 5 μs.

Edge Detection. The Sobel edge operator is estimated to take approximately 250 μs assuming a table look-up without interpolation scheme is used for finding the square root.

Feature Extraction. The feature extraction algorithm to extract the location of the towers in the oil rigs entails a conditional jump followed by a memory store. This would take about 2 μs.

Assuming that these five operations have to be performed over an image size of 206 by 286, the total processing time/frame is estimated to be 15 seconds. Adding 100% overhead time for setting up loops and memory to register transfers means that the overwater image can be processed and displayed in approximately 30 seconds. This processing time is clearly unacceptable. There are two possible ways of improving this time:

1. The point and spatial operations defined above are ideally suited for processing on an array processor (e.g., FPS-64). Such processors can provide an order of magnitude improvement in processing times.

2. Since the oil rig occupies a very small portion of the entire image, it is obvious that processing time can be reduced substantially if the target region can be tracked by some means. Assuming that a fix can be maintained on the target and the target region occupies a 50 x 100 pixel segment of the overall image, the processing time can be reduced to 1.3 seconds. However, the processing time for tracking the oil rig

has to be considered. This time obviously depends on the sophistication of the tracking algorithm. Radar images are updated (sweep time) approximately every one second. Thus, improvements in computer technology and hardware should make it possible to perform overwater image enhancement in periods of less than one second.

5. OVERLAND RADAR IMAGE ENHANCEMENT

The Petroleum Helicopter Inc. (PHI) heliport in Venice, La., shown in Figure 2, was used in gathering the overland radar image data for this study. The scene consists of a central building structure, a parking lot (full of cars), lakes in the rear, and several helicopters parked on a row of helipads in front of the building. Several radar images of this area were obtained with a radar antenna mounted in a helicopter (in the side-looking mode) that flew circular paths around the central building. The sum(S) radar image shown in Figure 6 has a cluster of bright pixels in the middle along with a dozen or more isolated bright pixels in its vicinity. As such, this image does not have much information that can be used by a pilot for navigation purposes, even if it is assumed that the pilot has prior knowledge of this scenario under visual flight conditions. Only after someone has seen this scene or its photograph (as given in Figure 2), does it make sense to give semantic meaning to the observed radar image data. Thus, after seeing both the radar and photographic images, it is possible to recognize some meaningful objects and terrain features; for example, one can "see" the building structure corresponding to the bright pixel cluster, the three helicopters on the right represented by the three bright isolated spots, and if one tries, the parking lot to the left of the building structure outlined by the roads.

For completeness, the individual even (E) and odd (O) images that comprise the sum(S) image of Figure 6 are included here as Figures 30 and 31, respectively. Notice that the odd image is relatively brighter than the even image. However, neither of these two images has any more information than what is contained in the sum image. Based upon the even, odd and sum radar images, it is fair to conclude that substantial improvements in image quality through application of image enhancement procedures would be required for these data to be meaningful for the pilot's navigation and guidance tasks.

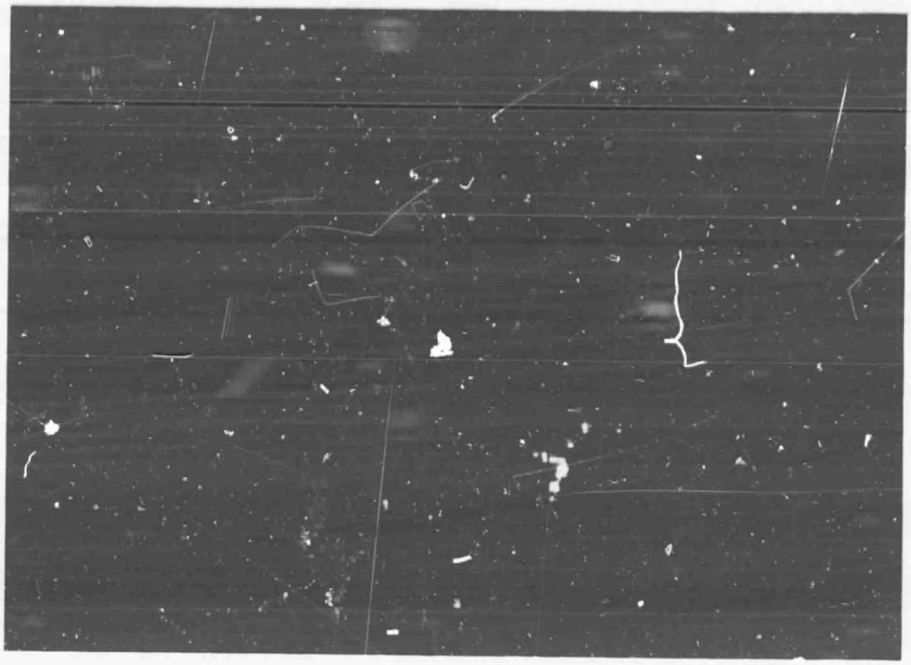

Figure 30. Overland Even Radar Image

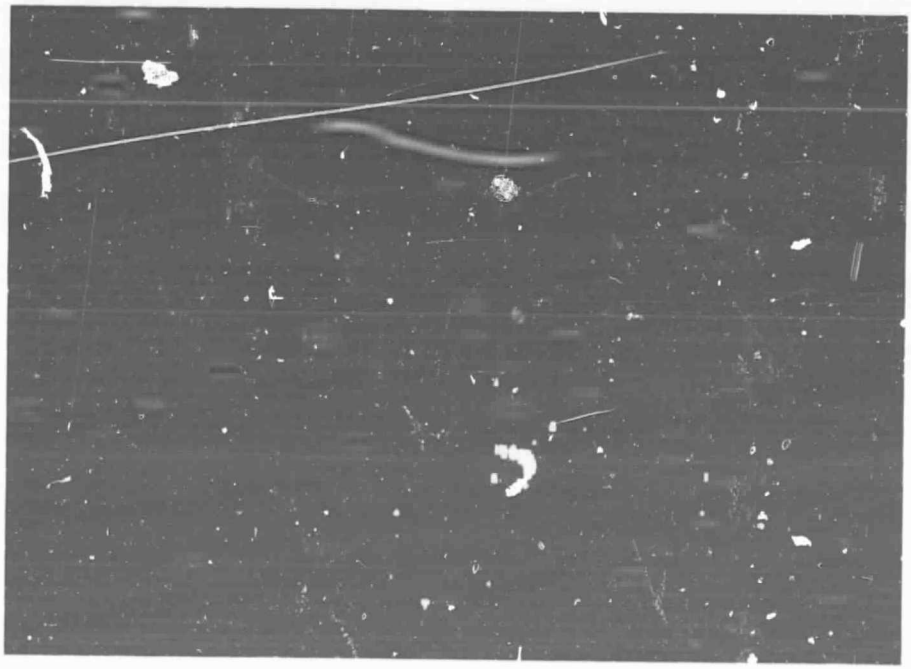

Figure 31. Overland Odd Radar Image

5.1 Characteristics of Overland Radar Images

Histogram of the radar image data were obtained to analyze the grey scale distribution of the pixel intensities. Figures 32-34 show the histograms for the original even, odd and sum radar images shown in Figures 30, 31 and 6, respectively. A look at these histogram shows that more than 50% of the pixels in each of these images have a pixel value that is less than 10 on an 8-bit (i.e. levels 0-255) image display. In other words, 50% or more of the image pixels are distributed exponentially over the lower (or 3-bit) 4% of the grey scale, while the remaining 50% or fewer pixels are uniformly distributed and cover the higher 96% of the dynamic range.

Clearly, the most obvious approach towards enhancing these radar images is to apply contrast stretching and manipulation algorithms to these data. The following section presents the results obtained using image enhancement methods.

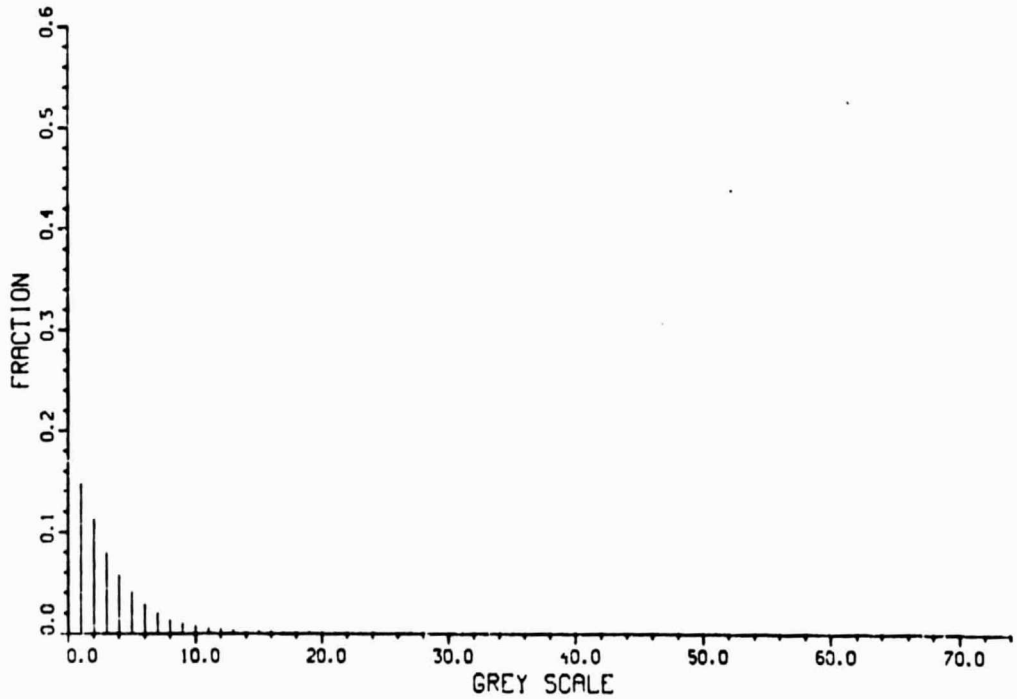

Figure 32. Histogram of Overland Even Radar Image

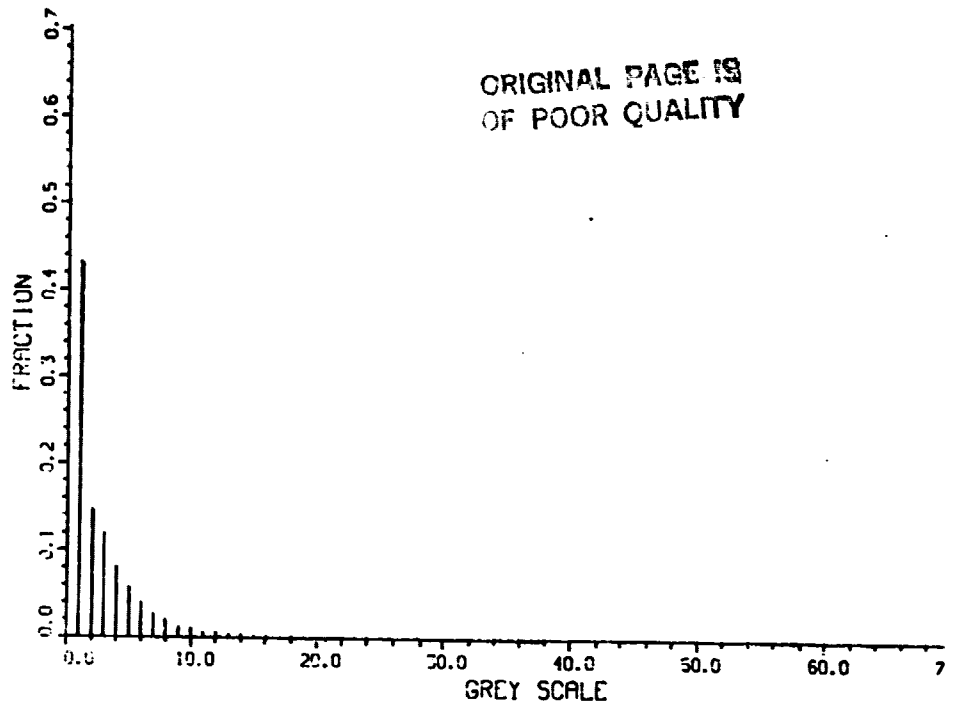

Figure 33. Histogram of Overland Odd Radar Image

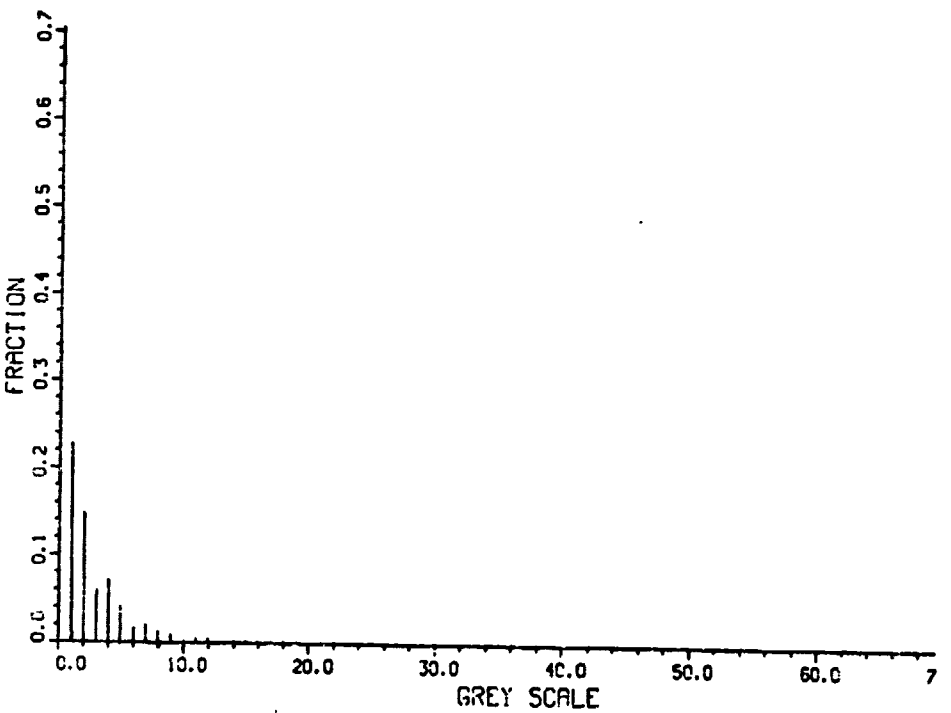

Figure 34. Histogram of Overland Sum Radar Image

5.2 Enhancement of Overland Radar Images

The objective of overland radar image enhancements is to manipulate the original image such that the processed image contains visual cues that are useful to the pilot's flight navigation and guidance task. For the scenario shown in Figure 2, the goal is to produce an enhanced radar image which shows the key features of the scene: namely, the building structure, the connected helipads, helicopters, the cars in the parking lot, the roadways surrounding the area, the lakes and other recognizable terrain features. In other words, the purpose of image enhancement is to modify the original radar images to appear, as much as possible, like the visual images seen by human eyes or the photographic camera, under clear visibility conditions.

As mentioned earlier, the original radar images have a grey scale distribution that is extremely skewed towards the lower pixel values (i.e. grey levels 0-10). Several point operations described in Section 2 such as the linear scaling function (as in Table 2), the piecewise linear and logarithmic contrast transformation operations (a and b in Table 3), and histogram equalization (Section 3.1.3) were investigated. Results from this study show that histogram equalization did not provide much improvement in the image quality, as compared to the piecewise linear and nonlinear contrast manipulation algorithms.

As a first step, a two-segment contrast transformation operator as shown in Figure 35 (not to scale) was applied to the sum radar image of Figure 6. This transformation stretches the constrast of the input image in the region from (0-10) to a range of (0-150) in the output image. Conversely, input image contrast from (10-255) is compressed to a smaller range of (150-255) in the enhanced image. Results of this contrast stretch/shrink operation on the sum image are shown in Figure 36. Comparing this enhanced image with the original image of Figure 6, it is apparent that significant improvements in the semantic content are obtained. The enhanced image of Figure 36 shows the building structure as in Figure 6, but more importantly brings out the general shape of the parking lot (including cars), the roadways (especially on the lower left at an angle of 60 degrees to the horizontal), and the helicopters on the right.

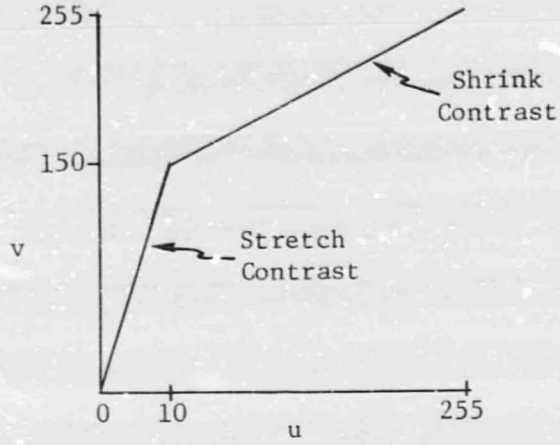

Figure 35. Two Segment Contrast Transformation Operator

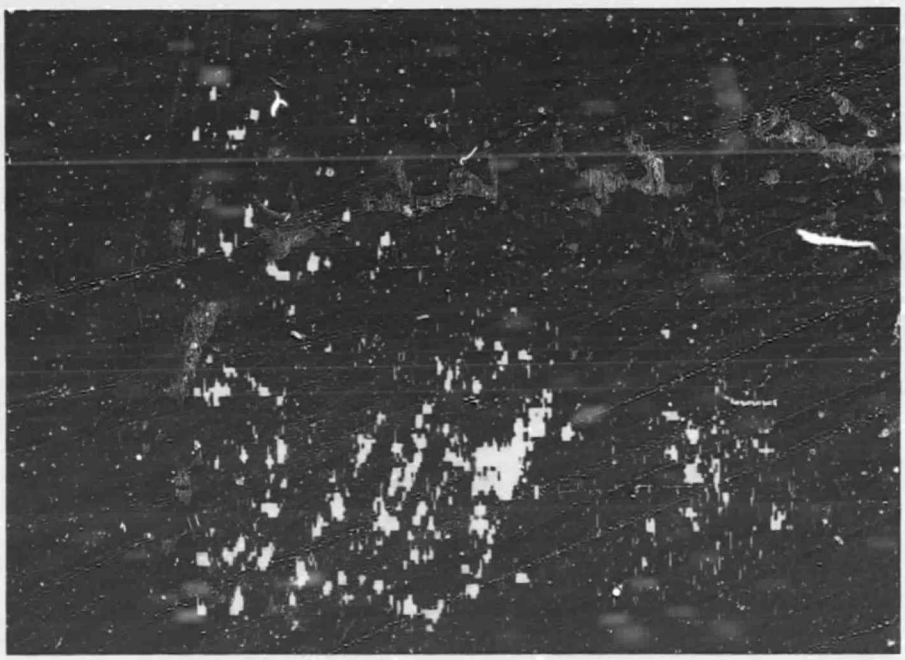

Figure 36. Enhanced Overland Sum Radar Image Obtained Using a Two-Segment Contrast Stretch/shrink operator

Further experiments with this transformation showed that additional improvement in picture quality may be obtained using a multiple segment contrast transformation operator, especially over the low intensity region of (0-10) in the input image. Instead, a continuous logarithmic transformation was applied to the sum image of Figure 6 (after transforming all the zero pixel values to one). The resulting image, log s*,

where: $s^* = 1 : u(m,n) = 0$

$u : u(m,n) \neq 0$

is shown in Figure 37. Notice that the logarithmically enhanced sum image of Figure 37 has significantly reduced the amount of impulse noise (i.e. isolated bright pixels) when compared to the two segment operator-enhanced image of Figure 36. A histogram of the log s* image is given in Figure 38. Note that the effect of the logarithm transform operation is to stretch the contrast of the processed image in the low intensity range by a factor of 7.

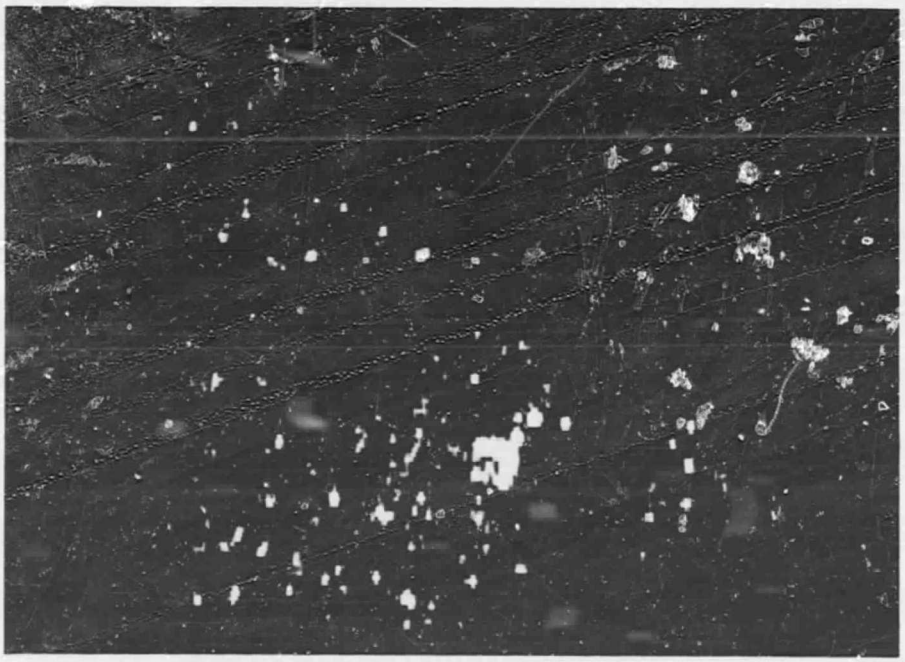

Figure 37. Logarithmically Enhanced Overland Sum Radar Image: log s^*

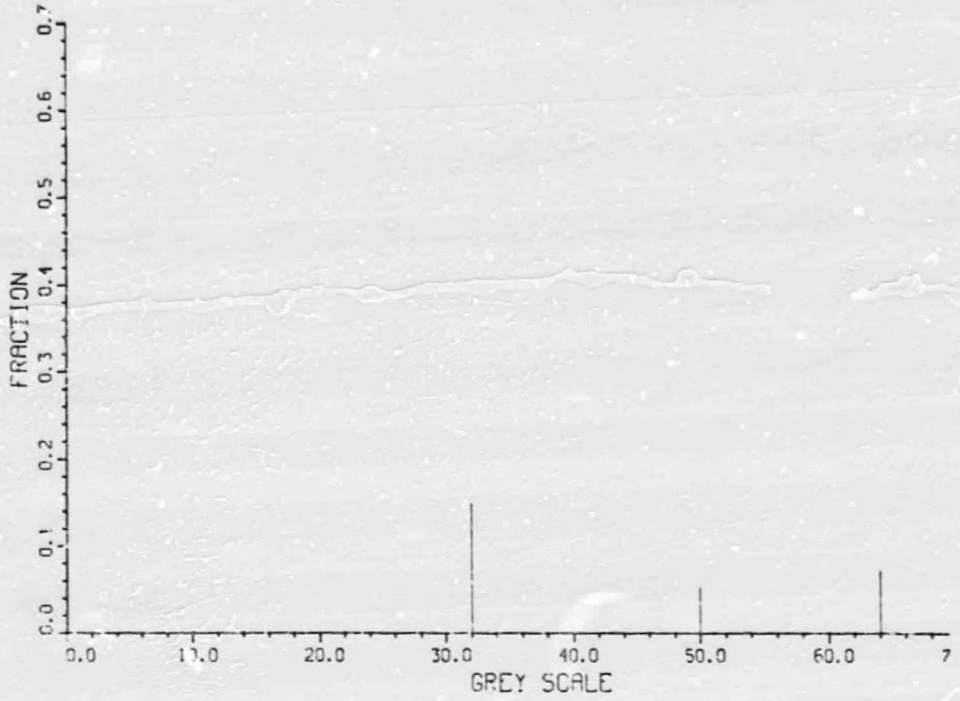

Figure 38. Histogram of Logarithmically Enhanced Overland Radar Sum Image

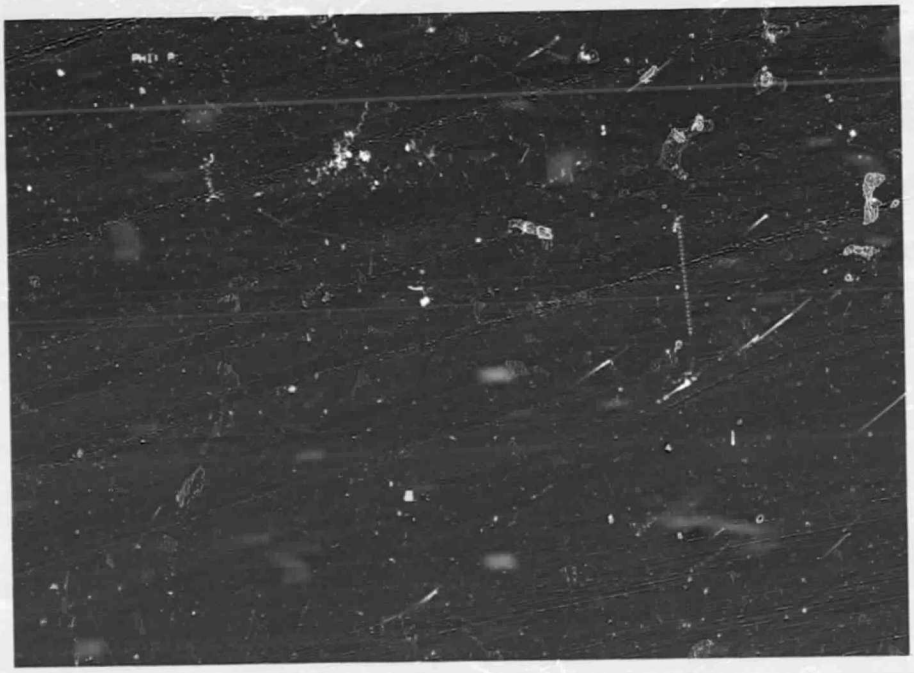

Figure 39. Product Image $P \equiv (E+1) \cdot (O+1)$

Finally, the logarithmic transformation was applied to the product of the even and odd images. The product image P = (E+1)(O+1) after rescaling to the (0-255) range is shown in Figure 39. Notice that the P image only shows a few bright pixels with a dark background. A histogram of the product image is shown in Figure 40. The product operation enhances pixel locations whose intensities are high in both the even and odd images. In other words, the

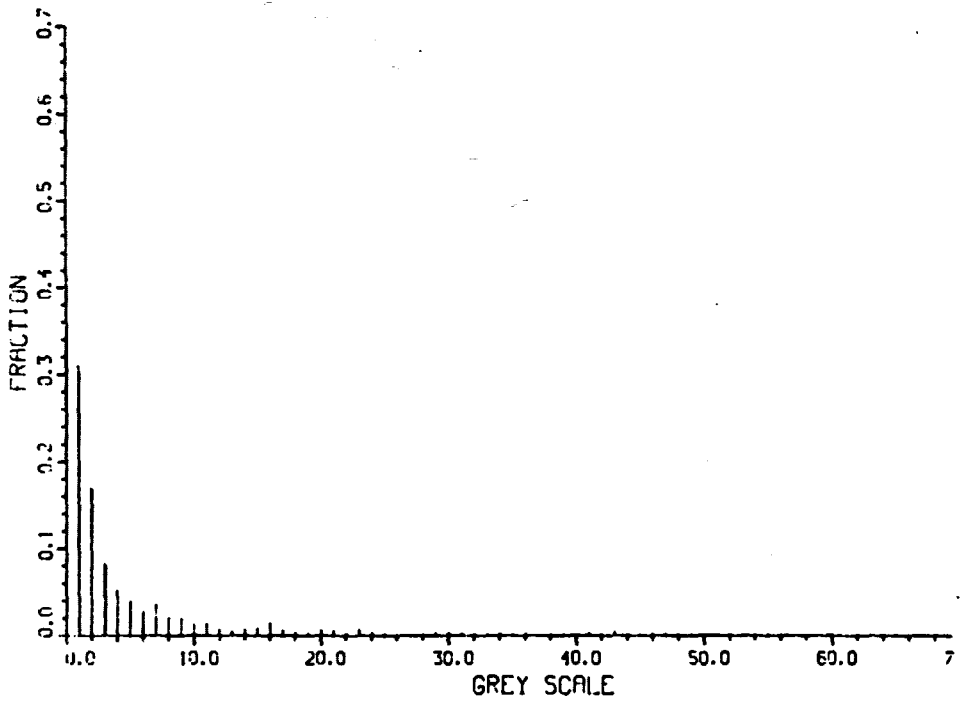

Figure 40. Histogram of Product Image

product operation enhances only those pixels in the even and odd images which are spatially correlated or registered. The log P image after rescaling to the (0-255) range is shown in Figure 41. This image shows a much better Figure 41 contrast and signal to noise ratio in comparison to the log s* image of Figure 37. A histogram of the log P image is shown in Figure 42. An examination of the product image (P) histogram in Figure 40 shows that approximately 75% of the product image pixels are exponentially distributed over the range (0-12) while the remaining 25% pixels are uniformly distributed

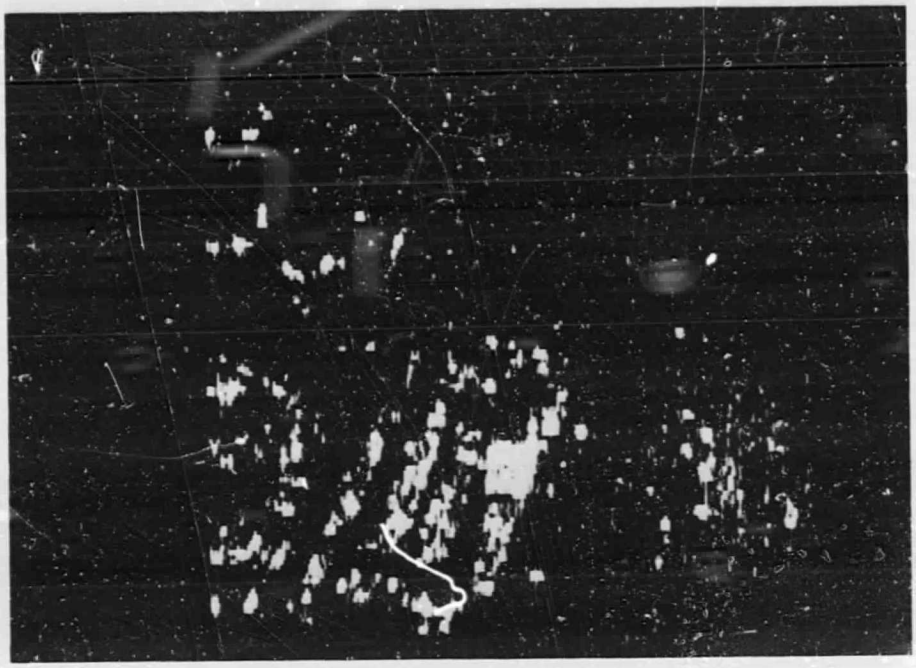

Figure 41. Logarithmically Enhanced Produce Image: log P

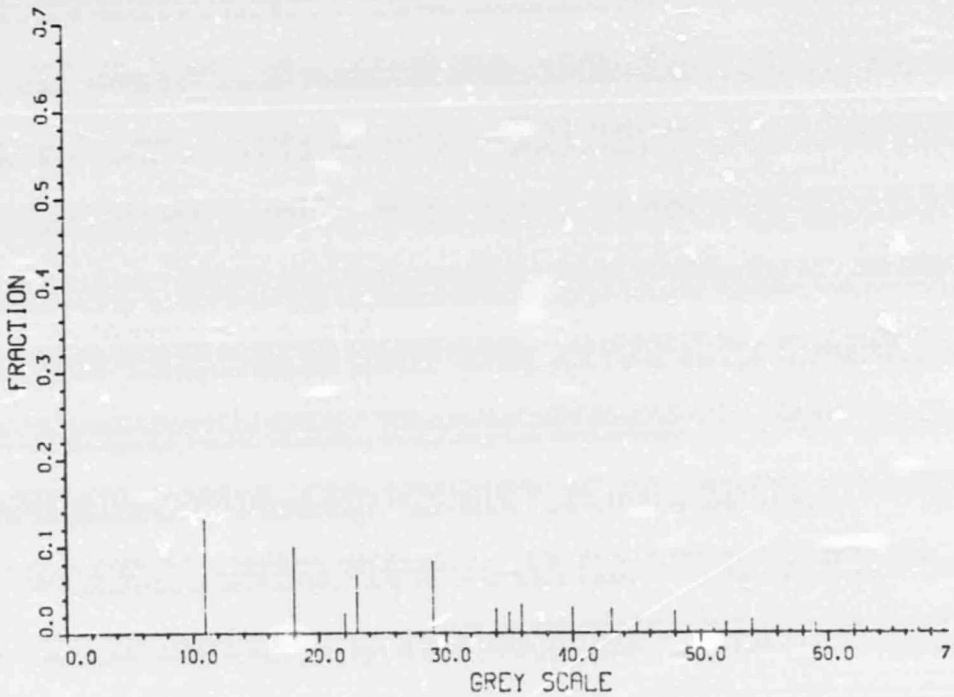

Figure 42. Histogram of Log P Image

over the grey levels (12-255). A decomposition of the logarithmic image log P into two images (1) a background or clutter image and (2) a foreground or target image can be accomplished by passing the original image through the two complementary filters shown in Figures 43(a) and (b), respectively.

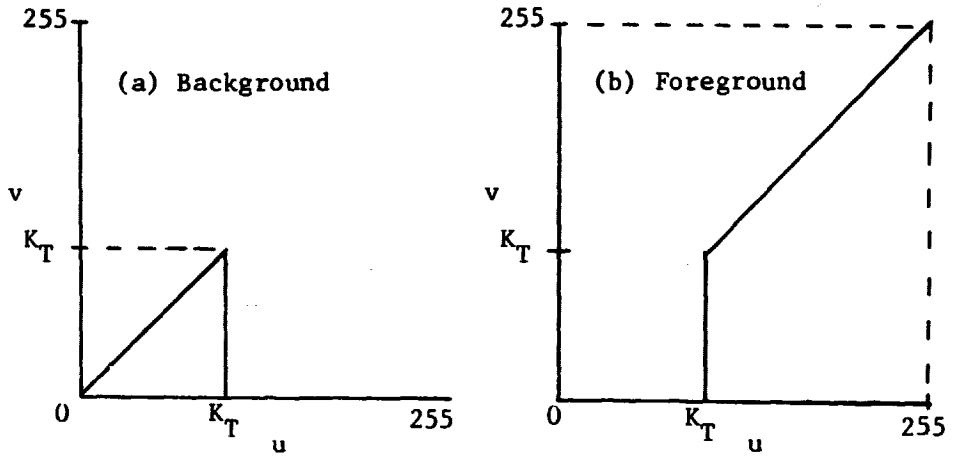

Figure 43. Decomposition Transformation for Background and Foreground Images

The threshold value K_T=50 was chosen for the log P image corresponding to the grey level threshold of 12 for the scaled product image P. Figures 44 and 45 show the background clutter and foreground target images. It is interesting to note that the original image log P in Figure 41 appears to have more information (from a subjective viewpoint) than the individual background and foreground images. The human eye seems to fill in the information (e.g. the perceived roadways) when the two image components are fused together. In other words, this example provides an illustration of the Gestalt viewpoint which states that "the sum is more than its parts."

Additional improvements to the contrast-enhanced image of Figure 41 may be possible through the application of spatial and edge detection algorithms, described earlier in Sections 3.2 and 3.3, respectively. However, experiments with these algorithms showed no significant improvements over the enhanced

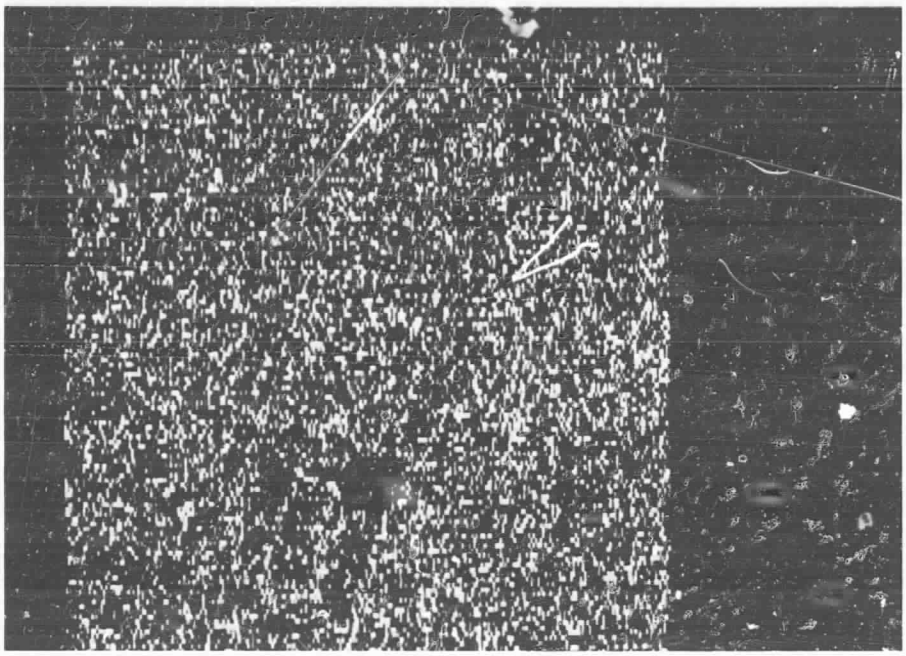

Figure 44. Background Clutter Image

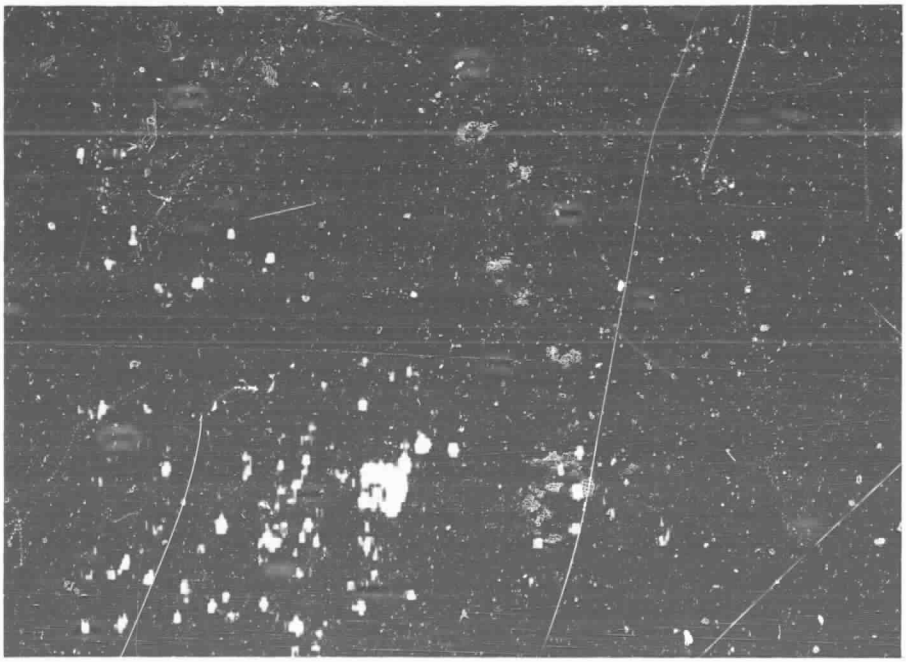

Figure 45. Foreground Target Image

image in Figure 41. The only operator which shows promise was the local area standard deviation operator.

Figures 46 and 47 show the images $\sigma_{logP}(2X2)$ and $\sigma_{logP}(3X3)$ corresponding to the standard deviation of the log P image over a (2X2) and (3X3) window, respectively. This operation enhances those portions of the log P image which have a large variability over a local area. The result is a sharpened image which displays distinct boundaries between foreground target area and background clutter. The size of the windows over which the standard deviation is computed must be adjusted on a case-by-case basis to provide a subjectively pleasing quality to the processed image.

Finally, Figure 48 shows a composite image consisting of 4 images arranged in a (2X2) matrix format. The individual elements are as follows:

(1X1) element = sum image(S) : Figure 6

(1X2) element = $\sigma_{logP}(2X2)$: Figure 45

(2X1) element = $\sigma_{logP}(3X3)$: Figure 46

(2X2) element = logP : Figure 41

Various other component images can be developed to illustrate and compare the results of different algorithms. Note that the image enhancement obtained using the alternate even and odd radar images is due to the increased signal to noise ratio resulting from adding or multiplying two almost registered images of the same target area. In other words, the improvement in image quality should not be attributed to the polarization difference between the even and odd image frames. Similar results would be expected without the use of alternating polarized pulses.

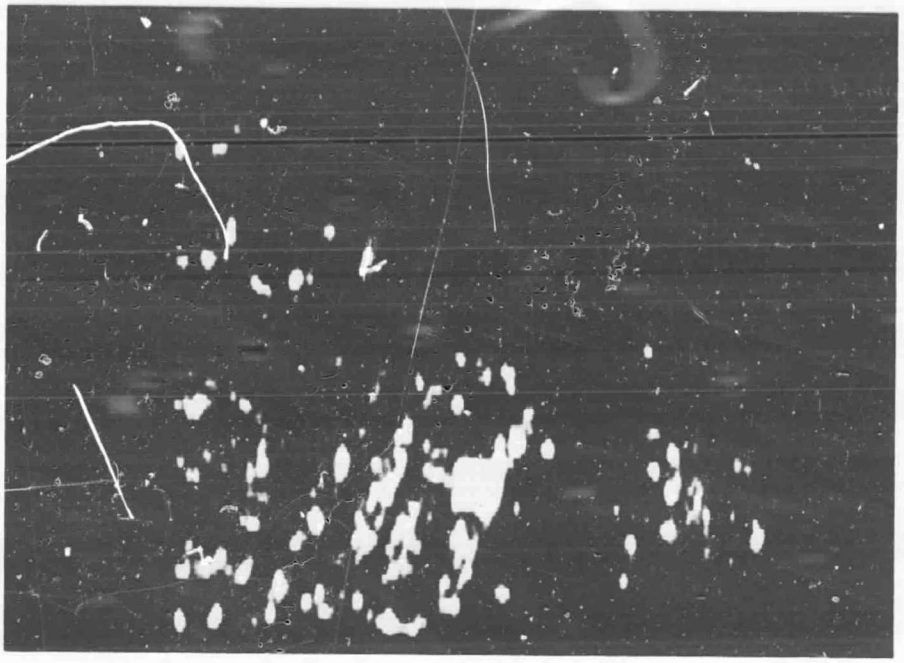

Figure 46. $\sigma_{\log P}(2 \times 2)$ Operator Enhanced Image

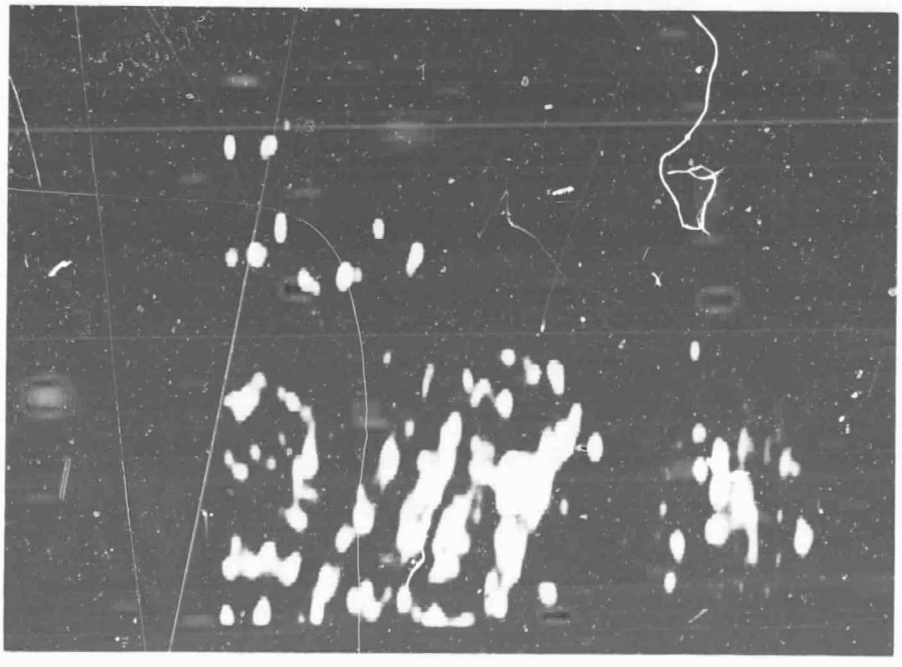

Figure 47. $\sigma_{\log P}(3 \times 3)$ Operator Enhanced Image

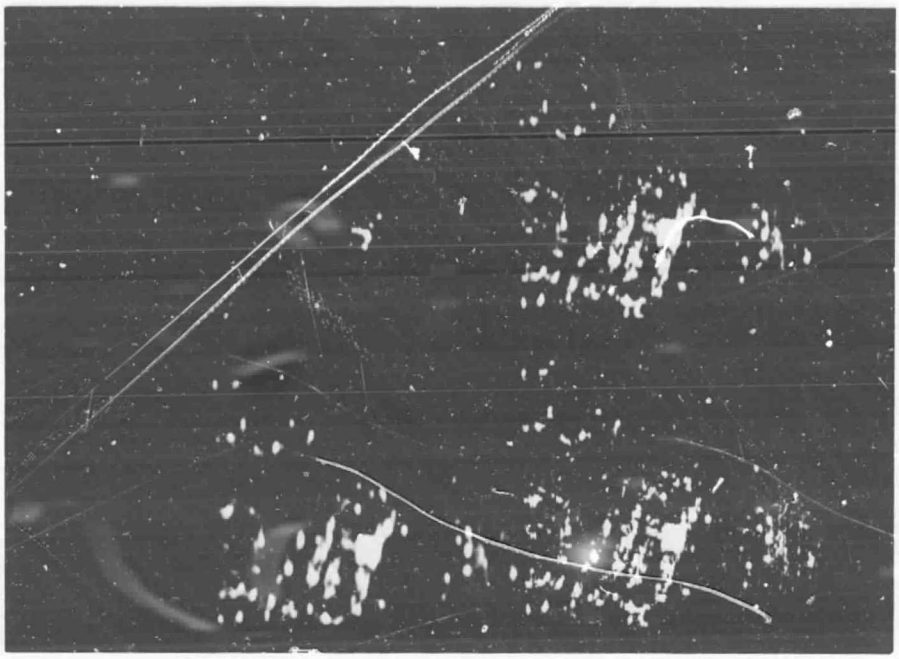

Figure 48. Composite of 4 Enhanced Images

5.3 Feasibility of Processing in Real-Time

The overland radar images can be enhanced significantly by taking the logarithm of the product of the horizontal and vertical polarized images. Assuming that a table look up algorithm is used to compute the logarithm, the processing time/pixel is estimated to be 13 μs. Assuming an image size of 206 x 286 pixels, the processing time would be approximately .8 secs. If 100% overhead time is assumed, the complete processing and display time for the contrast enhnacement of the overland image would take about 1.6 s. This time can be reduced by an order of magnitude if an array processor is used. Thus, near real-time implementation of the overland radar image enhancement algorithms is technically feasible at the present time.

6. CONCLUSIONS

The results of this study show that significant improvements in the raw millimeter radar images may be obtained using appropriate image enhancement algorithms. However, since the choice of the image enhancement algorithms is strongly dependent upon the nature of the target scenario and the image characteristics desired by the pilot, practical implementation of these algorithms would require considerable further research.

Radar images corresponding to two target-scenarios: an overwater oil rig scenario and an overland heliport site - were investigated. The overwater scene consists of an oil rig (two platforms with towers connected together by a catwalk) and a tugboat in the Gulf of Mexico. The radar image of this scene has a visible target area corresponding to the oil rig and the tugboat which is small in comparison to the remainder of the image which represents the ocean clutter. This study shows that it is possible to remove the ocean clutter and extract the target boundary as well as the tower and catwalk locations using a sequence of thresholding, binarization, median filtering and edge detection algorithms, in that order. The resulting image has only 2 grey levels. The image contains information in a manner that is more easily used by the pilot during navigation and obstacles avoidance than the original 64 grey level image. The consistency of these algorithms was verified by application to a sequence of three images.

The Petroleum Helicopter, Inc. (PHI) heliport site was used for overland radar image enhancement. The raw radar images are characterized by an extremely skewed statistical distribution of pixel values. As a result, the raw radar image has a few bright-pixel clusters over a dark background. This study shows that overland radar images for the PHI heliport scenario may be processed using nonlinear contrast stretching operations on the product of the two (even and odd) images obtained from the alternating pulse returns to produce an enhanced image where the details in the scene such as the buildings, the parking lot with cars, the roadways and helicopters on the pads are visible and identifiable to a trained operator.

A timing analysis of the radar image enhancement algorithms proposed for the overwater and overland scenarios shows that near real-time (i.e., processing time less than one frame period) implementation, using special purpose array processors, is technically feasible at the present time.

Based upon the success of this preliminary investigation, additional effort on techniques for further improving the quality of the enhanced radar images is warranted. This is particularly recommended for overland radar images where application of advanced methods based upon texture enhancement (e.g., using second and higher order distribution functions), shape detection operators (e.g., Hough transforms) and connectivity algorithms can greatly improve the contextual information content (e.g., improved delineation of roadways, marshland and other terrain background features) and perceptual quality of the enhanced images.

REFERENCES

1. Pratt, William K., **Digital Image Processing,** Wiley-Interscience, 1978.

2. Rosenfeld, Azriel and Kak, Avinash, C., **Digital Picture Processing,** Academic Press, 1976.

3. Hall, Ernest L., **Computer Image Processing and Recognition.** Academic Press, 1979.

4. Gonzalez, R. C. and Wintz, P. A., **Digital Image Processing,** Addison-Wesley, 1977.

5. Duda, R. O. and Hart, P. E., **Pattern Classification and Scene Analysis.** Wiley-Interscience, 1973.

6. Huang, T. S., Yang, G. J. and Tang, G. Y., **Fast Two-Dimensional Median Filtering Algorithm,** IEEE Transaction on Acoustics, Speech and Signal Processing, Vol. ASSP-27, No. 1, Feb. 1979.